Electronic Transactions on Numerical Analysis.
Volume 46, pp. 1–xx, 2019.

ISSN 1068–9613.

ETNA
Kent State University and
Johann Radon Institute (RICAM)

OPTIMIZED SURFACE PARAMETERIZATIONS WITH APPLICATIONS ON CHINESE VIRTUAL BROADCASTING*

MEI-HENG YUEH†, HSIAO-HAN HUANG‡, TIEXIANG LI§, WEN-WEI LIN‡, AND SHING-TUNG YAU¶

Abstract. Surface parameterizations have been widely applied in the computer-aided design for the geometric processing tasks of surface registration, remeshing, texture mapping, and so on. In this paper, we present an efficient balanced energy minimization algorithm for the computation of simply connected open surface parameterizations with balanced angle and area distortions. The existence of a nontrivial accumulation function of the proposed algorithm is guaranteed under some mild conditions and the limiting function is shown to be one-to-one. Comparisons of the proposed algorithm with the angle- and the area-preserving parameterizations show that the angular distortion is close to that of the angle-preserving parameterization while the area distortion is significantly improved. An application of the proposed algorithm on the Chinese virtual broadcasting technique is demonstrated thereafter, which is consisted of surface remeshing, registration, and morphing.

Key words. surface parameterization, simply connected open surface, balanced energy minimization, virtual broadcasting

AMS subject classifications. 15B48, 52C26, 65F05, 68U05, 65D18

1. Introduction.

A surface parameterization refers to a homeomorphism between the surface and the domain in $\mathbb{R}^2$ with a canonical shape. The parameterization can be used to induce a canonical coordinate system on the surface. The surface parameterization issue aims to develop a feasible algorithm for the computation of an ideal mapping that maps a given surface bijectively to a domain of a specified shape. This issue has been widely studied and applied in various tasks of computer vision, such as surface registration, remeshing, morphing, alignment, and texture mapping. More details on the history and recent advances for surface parameterization algorithms and applications can be found in survey papers [22, 49, 32, 10, 25, 29].

A good parameterization usually preserves as much geometric information as possible. In the past, most of the related works consider either angle-preserving (conformal) or area-preserving (equiareal) parameterizations. In practice, an ideal global parameterization of a simply connected open surface usually has a canonical shape, e.g., a disk or a rectangle, with both angle and area distortions being small.

We first briefly introduce related previous works on computational algorithms of surface parameterizations. An ideal parameterization usually preserves geometric structure of data to the utmost. The major classifications of surface parameterizations are based on conformal mappings, equiareal mappings, and mappings with balanced angle and area distortions.

A conformal parameterization targets to minimize the angle distortion. Varieties of feasible numerical algorithms have been proposed, including the linear Laplace-Beltrami equation [11, 30], the angle-based flattening [47, 48, 60], the discrete conformal parameterization [20], the least-squares conformal mapping [39], the holomorphic one-form method [27, 28, 36], the discrete conformal equivalence [50], the nonlinear heat diffusion [26, 33], the spectral conformal parameterization [43, 34], the discrete Ricci flow [35, 61], the fast landmark aligned spherical harmonic algorithm [17], the fast disk mapping [18], the orbifold Tutte embedding [7, 8, 6], the linear disk mapping [15], the conformal energy minimization [58], and the discrete Calabi flow [62].

*Received... Accepted... Published online on... Recommended by....
†Department of Mathematics, National Taiwan Normal University, Taipei, Taiwan (yue@ntnu.edu.tw).
‡Department of Applied Mathematics, National Chiao Tung University, Hsinchu, Taiwan.
§School of Mathematics, Southeast University, Nanjing, China.
¶Department of Mathematics, Harvard University, Cambridge, MA 02138, USA.

ETNA
Kent State University and
Johann Radon Institute (RICAM)

In contrast, an equiareal parameterization targets to minimize the area distortion. Several feasible numerical algorithms have been proposed, including the stretch-minimizing method [45, 55], the Lie advection method [64], the discrete optimal mass transportation [63, 52, 51], the density-equalizing mapping [16], and the stretch energy minimization [59, 57].

Furthermore, a distortion-balancing parameterization aims to reach a trade-off between minimizing the angle and area distortions. Some feasible numerical algorithms have been proposed, including the as-rigid-as-possible surface parameterization [40, 53], the most isometric parametrization [31, 19], the isometric distortion minimization [44], and the boundary first flattening [46].

Contribution. In this paper, we focus on developing an efficient balanced energy minimization (BEM) algorithm for the computation of an optimized surface parameterization that maps a simply connected open surface to the unit disk with balanced angle and area distortions. In BEM algorithm, we use the golden section search and parabolic interpolation [13, 23] to find the best balancing coefficient β^*. For a given balancing coefficient β in each step, we update the balanced Laplacian matrix and compute an approximate parameterization between the surface and the unit disk until convergence. (See Algorithm 1 for details.) In addition, we prove the existence of a nontrivial accumulation function of the BEM algorithm under the assumption that the given mesh is a Delaunay triangulation, and the bijectivity of the limiting function. A comparison of the BEM algorithm with the angle- and the area-preserving parameterizations shows that the angle distortion is close to that of the angle-preserving parameterization while the area distortion is significantly improved. With the disk-shaped balanced parameterizations, the one-to-one correspondence, i.e., the registration mapping, between surfaces can be easily computed on the unit disk so that the morphing and alignment between surfaces can be smoothly handled. We then apply the BEM algorithm to develop a Chinese virtual broadcasting technique, which is consisted of surface remeshing, registration and morphing skills.

This paper is organized as follows. First, in Section 2 we propose an efficient BEM algorithm for computing the optimal distortion-balancing surface parameterization. In Section 3, we prove the existence of nontrivial accumulation function of the BEM algorithm and show the limiting function is one-to-one. Numerical experiments and comparisons of our optimal distortion-balancing parameterizations with the conformal and equiareal parameterizations are presented in Section 4. The application of the distortion-balancing parameterizations on Chinese virtual broadcasting is demonstrated in Section 5. A concluding remark is given in Section 6.

2. Balanced Energy Minimization Algorithm. The following notations are used in this paper, other notations will be clearly defined when they appear.

- Bold letters, e.g. $\mathbf{u}$, $\mathbf{v}$, $\mathbf{w}$, denote (complex) vectors.
- Capital letters, e.g. A, B, C, denote matrices.
- Typewriter letters, e.g. $\mathtt{I}$, $\mathtt{J}$, $\mathtt{K}$, denote ordered sets of indices.
- $n_{\mathtt{I}}$ denotes the number of elements in the set $\mathtt{I}$.
- $\mathbf{v}_i$ denotes the ith entry of the vector $\mathbf{v}$.
- $\mathbf{v}_{\mathtt{I}}$ denotes the subvector of $\mathbf{v}$ composed of $\mathbf{v}_i$, for $i \in \mathtt{I}$.
- $|\mathbf{v}|$ denotes the vector with the ith entry being $|\mathbf{v}_i|$.
- $\operatorname{diag}(\mathbf{v})$ denotes the diagonal matrix with the (i,i)th entry being $\mathbf{v}_i$.
- $A_{i,j}$ denotes the (i,j)th entry of the matrix A.
- $A_{\mathtt{I},\mathtt{J}}$ denotes the submatrix of A composed of $A_{i,j}$, for $i \in \mathtt{I}$ and $j \in \mathtt{J}$.
- $\mathbb{D} := \{z \in \mathbb{C} \,|\, |z| \leq 1\}$ denotes the unit disk in $\mathbb{C}$.
- i denotes the imaginary unit $\sqrt{-1}$.
- I_n denotes the identity matrix of size $n \times n$.

ETNA
Kent State University and
Johann Radon Institute (RICAM)

- $\mathbf{1}_n$ denotes the vector of length n with all the entries being 1.
- $\mathbf{0}$ denotes the zero vectors and matrices of appropriate sizes.

In this paper, we consider simply connected open discrete surfaces embedded in $\mathbb{R}^3$. A discrete surface $\mathcal{M}$ refers to a triangular mesh (homogeneous simplicial 2-complex) composed of n vertices with coordinates in $\mathbb{R}^3$

$$\mathcal{V}(\mathcal{M}) = \left\{ v_s \equiv \left(v_s^1, v_s^2, v_s^3\right)^\top \in \mathbb{R}^3 \right\}_{s=1}^{n},$$

triangular faces

$$\mathcal{F}(\mathcal{M}) = \left\{ [v_i, v_j, v_k] \subset \mathbb{R}^3 \text{ for some vertices } \{v_i, v_j, v_k\} \subset \mathcal{V}(\mathcal{M}) \right\},$$

and edges

$$\mathcal{E}(\mathcal{M}) = \left\{ [v_i, v_j] \mid [v_i, v_j, v_k] \in \mathcal{F}(\mathcal{M}) \text{ for some } v_k \in \mathcal{V}(\mathcal{M}) \right\}.$$

The bracket $[v_i, v_j, v_k]$ denotes the *convex hull* of the affinely independent vertices $\{v_i, v_j, v_k\}$.

On the other hand, a discrete mapping $f : \mathcal{M} \to \mathbb{C}$ is a piecewise affine mapping, i.e., for each triangular face $\tau \in \mathcal{F}(\mathcal{M})$, the restriction mapping $f|_\tau : \tau \to \mathbb{C}$ is an affine mapping which can be represented as a complex-valued vector

$$\mathbf{f} = (f(v_1), \cdots, f(v_n))^\top \in \mathbb{C}^n.$$

For a point $v \in [v_i, v_j, v_k] \in \mathcal{F}(\mathcal{M})$, the value $f(v)$ is defined as

$$f(v) = f|_{[v_i, v_j, v_k]}(v) = \lambda_i(v)\, \mathbf{f}_i + \lambda_j(v)\, \mathbf{f}_j + \lambda_k(v)\, \mathbf{f}_k,$$

where the coefficients $\lambda_i(v) = \frac{|[v, v_j, v_k]|}{|[v_i, v_j, v_k]|}$, $\lambda_j(v) = \frac{|[v_i, v, v_k]|}{|[v_i, v_j, v_k]|}$, and $\lambda_k(v) = \frac{|[v_i, v_j, v]|}{|[v_i, v_j, v_k]|}$ are known as the *barycentric coordinates* of v on $[v_i, v_j, v_k]$. Here the absolute value $|[v_i, v_j, v_k]|$ denotes the area of the triangular face $[v_i, v_j, v_k]$.

We now develop the BEM algorithm for the computation of disk-shaped surface parameterizations with balanced angle and area distortions. The strategy is to minimize a linear combination of the conformal energy [58] and the stretch energy [59]. First, we briefly review the conformal and stretch energy functionals in Section 2.1. Then, we introduce the distortion-balancing parameterization algorithm in Section 2.2.

2.1. Conformal and Stretch Energy Functionals [58, 59]. The discrete conformal energy of a discrete mapping $f : \mathcal{M} \to \mathbb{C}$ is defined as

$$E_C(f) = E_D(f) - \mathcal{A}(f),$$

where E_D is the discrete Dirichlet energy given by

$$E_D(f) = \frac{1}{2}\, \mathbf{f}^* L_D \mathbf{f}$$

in which L_D is the Laplacian matrix with

$$[L_D]_{i,j} = \begin{cases} -\frac{1}{2}(\cot\theta_{i,j} + \cot\theta_{j,i}) & \text{if } [v_i, v_j] \in \mathcal{E}(\mathcal{M}), \\ -\sum_{k \neq i} [L_D]_{i,k} & \text{if } j = i, \\ 0 & \text{otherwise,} \end{cases} \tag{2.1}$$

ETNA
Kent State University and
Johann Radon Institute (RICAM)

$\theta_{i,j}$ and $\theta_{j,i}$ are the angles opposite to the edge $[v_i, v_j]$ connecting vertices v_i and v_j on the mesh $\mathcal{M}$, and $\mathcal{A}(f)$ denotes the image area given by

$$\mathcal{A}(f) = \frac{1}{2} \sum_{[v_i,v_j]\in\partial\mathcal{M}} (\operatorname{Re}\mathbf{f}_i \operatorname{Im}\mathbf{f}_j - \operatorname{Re}\mathbf{f}_j \operatorname{Im}\mathbf{f}_i).$$

It is worth noting that when the shape of the image is given, e.g., a unit disk $\mathbb{D}$, the image area $\mathcal{A}(f)$ would be constant, so that minimizing E_C is equivalent to minimizing E_D.

On the other hand, the stretch energy of the discrete mapping $f : \mathcal{M} \to \mathbb{C}$ is defined as

$$E_S(f) = \frac{1}{2}\mathbf{f}^* L_S(f)\mathbf{f},$$

where $L_S(f)$ is the stretch Laplacian matrix with

$$[L_S(f)]_{i,j} = \begin{cases} -\frac{1}{2}\left(\frac{\cot(\theta_{i,j}(f))}{\sigma_{f^{-1}}([v_i,v_j,v_k])} + \frac{\cot(\theta_{j,i}(f))}{\sigma_{f^{-1}}([v_j,v_i,v_\ell])}\right) & \text{if } [v_i, v_j] \in \mathcal{E}(\mathcal{M}), \\ \sum_{k\neq i} -[L_S(f)]_{i,k} & \text{if } j = i, \\ 0 & \text{otherwise} \end{cases} \tag{2.2}$$

in which $\theta_{i,j}(f)$ and $\theta_{j,i}(f)$ are the angles opposite to the edge $f([v_i, v_j])$ connecting points $f(v_i)$ and $f(v_j)$ on the image $f(\mathcal{M})$ and

$$\sigma_{f^{-1}}([v_i, v_j, v_k]) = \frac{|[v_i, v_j, v_k]|}{|f([v_i, v_j, v_k])|}$$

is the stretch factor of f on the triangular face $[v_i, v_j, v_k]$.

2.2. Balanced Energy Minimization (BEM) Algorithm. The distortion-balancing parameterization algorithm aims to find a mapping $f : \mathcal{M} \to \mathbb{D}$ that minimize the balanced energy functional

$$E_\beta(f) = \frac{1}{2}\mathbf{f}^* L_\beta(f)\mathbf{f}$$

in which $L_\beta(f)$ is the balanced Laplacian matrix given by

$$L_\beta(f) = (1-\beta)\frac{L_D}{\|L_D\|_F} + \beta\frac{L_S(f)}{\|L_S(f)\|_F}, \tag{2.3}$$

where $\|\cdot\|_F$ denotes the Frobenius norm, β is the balancing coefficient in $[0, 1]$, L_D and L_S are Laplacian matrices defined as (2.1) and (2.2), respectively. The balanced Laplacian matrix in (2.3) is a convex combination of the normalized Laplacian matrices $\frac{L_D}{\|L_D\|_F}$ and $\frac{L_S(f)}{\|L_S(f)\|_F}$. In particular, when $\beta = 0$, the functional is equivalent to the Dirichlet energy E_D. Similarly, when $\beta = 1$, the functional is equivalent to the stretch energy E_S. In the following, for a given coefficient $\beta \in [0, 1]$, we introduce a numerical method for computing a mapping $f : \mathcal{M} \to \mathbb{D}$ that minimizes the balanced energy E_β.

The initial boundary mapping $f^{(0)}|_{\partial\mathcal{M}} : \partial\mathcal{M} \to \partial\mathbb{D}$ is computed by solving the discrete Laplace-Beltrami equation

$$L_D\mathbf{f}^{(0)} = \mathbf{b}, \tag{2.4}$$

ETNA
Kent State University and
Johann Radon Institute (RICAM)

where the vector $\mathbf{b} = (\mathbf{b}_1, \ldots, \mathbf{b}_n)^\top$ is given by

$$\mathbf{b}_k := \begin{cases} \frac{-1}{\|v_b - v_a\|_2} + \mathrm{i}\frac{1-\alpha}{\|v_c - (v_a + \alpha(v_b - v_a))\|_2} & \text{if } k = a, \\ \frac{1}{\|v_b - v_a\|} + \mathrm{i}\frac{\alpha}{\|v_c - (v_a + \alpha(v_b - v_a))\|_2} & \text{if } k = b, \\ \mathrm{i}\frac{-1}{\|p_c - (v_a + \alpha(v_b - v_a))\|_2} & \text{if } k = c, \\ 0 & \text{if } k \notin \{a, b, c\} \end{cases} \tag{2.5}$$

with $\alpha = \frac{\langle v_c - v_a, v_b - v_a \rangle}{\|v_b - v_a\|_2^2}$, the triangular face $[v_a, v_b, v_c]$ is the one closest to the mass center of $\mathcal{M}$. The equation (2.4) was first proposed by Angenent et al. [11, 30] for the computation of spherical harmonic mappings of genus-zero closed surfaces. It was modified by Yueh et al. [58] for the computation of disk-shaped harmonic mappings of simply connected open surfaces.

Let $\mathtt{I}$ and $\mathtt{B}$ be the ordered index sets of the interior and boundary vertices, respectively. The subvector $\mathbf{f}_\mathtt{B}^{(0)}$ in (2.4) defines a boundary mapping. To constrain the image of the boundary $\mathbf{f}_\mathtt{B}^{(0)}$ to be a unit circle, we perform the centralization

$$\mathbf{f}_\mathtt{B}^{(0)} \leftarrow \left(I_{n_\mathtt{B}} - \frac{\mathbf{1}_{n_\mathtt{B}} \mathbf{1}_{n_\mathtt{B}}^\top}{n_\mathtt{B}} \right) \mathbf{f}_\mathtt{B}^{(0)}$$

and the normalization

$$\mathbf{f}_\mathtt{B}^{(0)} \leftarrow \left(\operatorname{diag}\left(|\mathbf{f}_\mathtt{B}|\right)\right)^{-1} \mathbf{f}_\mathtt{B}^{(0)}.$$

Then the interior of the initial mapping is obtained by solving the linear system

$$[L_D]_{\mathtt{I},\mathtt{I}} \mathbf{f}_\mathtt{I}^{(0)} = -[L_D]_{\mathtt{I},\mathtt{B}} \mathbf{f}_\mathtt{B}^{(0)}. \tag{2.6}$$

Next, suppose a mapping $f^{(k)}$ at the kth step is obtained. In order to decrease the balanced energy E_β, we first compute the boundary of $f^{(k+1)}$ by solving the linear system

$$\left[L_\beta(f^{(k)})\right]_{\mathtt{B},\mathtt{B}} \mathbf{f}_\mathtt{B}^{(k+1)} = -\left[L_\beta(f^{(k)})\right]_{\mathtt{B},\mathtt{I}} \operatorname{diag}\left(\mathbf{f}_\mathtt{I}^{(k)}\right)^{-2} \mathbf{f}_\mathtt{I}^{(k)}. \tag{2.7}$$

Again, the circular boundary constraint is reached by performing the centralization

$$\mathbf{f}_\mathtt{B}^{(k+1)} \leftarrow \left(I_{n_\mathtt{B}} - \frac{\mathbf{1}_{n_\mathtt{B}} \mathbf{1}_{n_\mathtt{B}}^\top}{n_\mathtt{B}} \right) \mathbf{f}_\mathtt{B}^{(k+1)} \tag{2.8}$$

and the normalization

$$\mathbf{f}_\mathtt{B}^{(k+1)} \leftarrow \operatorname{diag}\left(|\mathbf{f}_\mathtt{B}|\right)^{-1} \mathbf{f}_\mathtt{B}^{(k+1)}. \tag{2.9}$$

Finally, the interior mapping is obtained by solving the linear system

$$\left[L_\beta(f^{(k)})\right]_{\mathtt{I},\mathtt{I}} \mathbf{f}_\mathtt{I}^{(k+1)} = -\left[L_\beta(f^{(k)})\right]_{\mathtt{I},\mathtt{B}} \mathbf{f}_\mathtt{B}^{(k+1)}. \tag{2.10}$$

The iteration is terminated until a certain maximum number of iterations is reached or the energy cannot be further decreased.

In fact, the Laplacian matrices L_D, $L_S(f)$, and $L_\beta(f)$ in (2.1), (2.2), and (2.3), respectively, are sparse symmetric positive semidefinite irreducible M-matrices. Consequently, their

ETNA
Kent State University and
Johann Radon Institute (RICAM)

principal submatrices are symmetric positive definite M-matrices. Then the linear systems (2.6), (2.7), and (2.10) can be solved by the Cholesky solver.

For a given $\beta \in [0,1]$, iterations (2.7)–(2.10) can compute the function $f_\beta : \mathcal{M} \to \mathbb{D}$ for minimizing the balanced energy $E_\beta(f)$, i.e., $f_\beta := \operatorname{argmin}_{f:\mathcal{M}\to\mathbb{D}} E_\beta(f)$. Here, the choice of the balancing value is crucial for applications. An optimal value of β can be determined by

$$\beta = \operatorname*{argmax}_{\beta\in[0,1]} g(\beta), \tag{2.11}$$

where $g(\beta) = \min_{f:\mathcal{M}\to\mathbb{D}} E_\beta(f)$ is a single-variable bounded function of β. The maximizer of (2.11) can be obtained by the built-in function `fminbnd` [13, 23] in MATLAB. The BEM algorithm for distortion-balancing parameterizations with the optimal value β^* is summarized in Algorithm 1.

Complexity of BEM. Denote

s_β : the number of iterations for the computation of β^* in Step 11 of the BEM algorithm,

s_g : the number of iterations for the while-loop in Step 21–35 of the BEM algorithm.

The dominate steps in the BEM algorithm are solving the linear systems of size $n_{\mathtt{I}}$ and $n_{\mathtt{B}}$ by Cholesky solver in Step 28 and 25, respectively. In practice, $n_{\mathtt{I}}$ is rather larger than $n_{\mathtt{B}}$. The complexity of BEM algorithm can then be estimated by

$$\text{Complexity(BEM)} = s_\beta s_g \left(\frac{1}{6} n_{\mathtt{I}}^3 + O(n_{\mathtt{I}}^2) + \frac{1}{6} n_{\mathtt{B}}^3 + O(n_{\mathtt{B}}^2) \right). \tag{2.12}$$

3. Existence of Nontrivial Accumulation Points for BEM. In this section, we prove the existence of a nontrivial (nonconstant) accumulation function of iterations (2.7)–(2.10) in the BEM algorithm. Then we show the limiting piecewise affine function is a one-to-one map. The iterations form a sequence $\{\mathbf{f}_{\mathtt{B}}^{(k)}\}_{k\in\mathbb{N}}$ given by

$$\mathbf{f}_{\mathtt{B}}^{(k+1)} = D_N^{(k)} C \left[L_\beta(f^{(k)})\right]_{\mathtt{B},\mathtt{B}}^{-1} \left[L_\beta(f^{(k)})\right]_{\mathtt{B},\mathtt{I}} D_V^{(k)} \left[L_\beta(f^{(k)})\right]_{\mathtt{I},\mathtt{I}}^{-1} \left[L_\beta(f^{(k)})\right]_{\mathtt{I},\mathtt{B}} \mathbf{f}_{\mathtt{B}}^{(k)}, \tag{3.1}$$

where $D_V^{(k)}$ is the inversion matrix given by

$$D_V^{(k)} = \operatorname{diag}\left(\left| \left[L_\beta(f^{(k)})\right]_{\mathtt{I},\mathtt{I}}^{-1} \left[L_\beta(f^{(k)})\right]_{\mathtt{I},\mathtt{B}} \mathbf{f}_{\mathtt{B}}^{(k)} \right| \right)^{-2},$$

C is the centralization matrix given by $C = I_{n_{\mathtt{B}}} - \frac{1}{n_{\mathtt{B}}} \mathbf{1}_{n_{\mathtt{B}}} \mathbf{1}_{n_{\mathtt{B}}}^\top$, and $D_N^{(k)}$ is the normalization matrix given by

$$D_N^{(k)} = \operatorname{diag}\left(\left| C \left[L_\beta(f^{(k)})\right]_{\mathtt{B},\mathtt{B}}^{-1} \left[L_\beta(f^{(k)})\right]_{\mathtt{B},\mathtt{I}} D_V^{(k)} \left[L_\beta(f^{(k)})\right]_{\mathtt{I},\mathtt{I}}^{-1} \left[L_\beta(f^{(k)})\right]_{\mathtt{I},\mathtt{B}} \mathbf{f}_{\mathtt{B}}^{(k)} \right| \right)^{-1}.$$

In order to prove the bijectivity of the parameterization, we give the *well-condition* assumption for the triangular mesh as follows.

DEFINITION 3.1 (Well-conditioned mesh). *A simply connected open mesh $\mathcal{M}$ is said to be* well-conditioned *if it satisfies the following conditions:*

(i) The subgraph of all the interior vertices is connected.

(ii) Every boundary vertex is connected to at least one interior vertex.

(iii) Both the numbers of interior and boundary vertices are larger or equal to 3.

ETNA
Kent State University and
Johann Radon Institute (RICAM)

Algorithm 1 Balanced Energy Minimization (BEM)

Input: A simply connected open mesh $\mathcal{M}$.
Output: A distortion-balancing parameterization $f_{\beta^*} : \mathcal{M} \to \mathbb{D}$ with the optimal value β^*.

1: **global variables**
2: $\mathcal{M}$: the input simply connected open mesh
3: $\mathbf{f}$: the parameterization
4: $\mathtt{I}$: the ordered index set of the interior vertices
5: $\mathtt{B}$: the ordered index set of the boundary vertices
6: L_D: the Laplacian matrix as defined in (2.1)
7: $L_S(\mathbf{f})$: the Laplacian matrix as defined in (2.2)
8: **end global variables**
9: **procedure** MAIN
10: $\mathbf{f} =$ INITIALMAPPING.
11: $\beta^* = \mathtt{fminbnd}(-g(\beta))$. ▷ `fminbnd` is a built-in function in MATLAB.
12: **return** $\mathbf{f}$. ▷ The global variable $\mathbf{f}$ is updated in line 10.
13: **end procedure**
14: **procedure** INITIALMAPPING
15: Solve $L_D\mathbf{f} = \mathbf{b}$, where $\mathbf{b}$ is as defined in (2.5).
16: $\mathbf{f}_\mathtt{B} \leftarrow (I_{n_\mathtt{B}} - \frac{1}{n_\mathtt{B}}\mathbf{1}_{n_\mathtt{B}}\mathbf{1}_{n_\mathtt{B}}^\top)\mathbf{f}_\mathtt{B}$. ▷ Centralize the boundary mapping $\mathbf{f}_\mathtt{B}$.
17: $\mathbf{f}_\mathtt{B} \leftarrow \operatorname{diag}(|\mathbf{f}_\mathtt{B}|)^{-1}\mathbf{f}_\mathtt{B}$. ▷ Normalize the boundary mapping $\mathbf{f}_\mathtt{B}$.
18: Solve $[L_D]_{\mathtt{I},\mathtt{I}}\mathbf{f}_\mathtt{I} = -[L_D]_{\mathtt{I},\mathtt{B}}\mathbf{f}_\mathtt{B}$. ▷ Update the interior mapping $\mathbf{f}_\mathtt{I}$.
19: **return** $\mathbf{f}$. ▷ $\mathbf{f}$ is the initial mapping.
20: **end procedure**
21: **procedure** $g(\beta)$
22: **while** not convergent **do**
23: $L \leftarrow (1-\beta)\frac{L_D}{\|L_D\|_F} + \beta\frac{L_S(\mathbf{f})}{\|L_S(\mathbf{f})\|_F}$. ▷ Update the balanced Laplacian matrix.
24: $\mathbf{h} \leftarrow \mathbf{f}$. ▷ Store the current mapping.
25: Solve $L_{\mathtt{B},\mathtt{B}}\mathbf{f}_\mathtt{B} = -L_{\mathtt{B},\mathtt{I}}\operatorname{diag}(|\mathbf{f}_\mathtt{I}|)^{-2}\mathbf{f}_\mathtt{I}$. ▷ Update the boundary mapping $\mathbf{f}_\mathtt{B}$.
26: $\mathbf{f}_\mathtt{B} \leftarrow (I_{n_\mathtt{B}} - \frac{1}{n_\mathtt{B}}\mathbf{1}_{n_\mathtt{B}}\mathbf{1}_{n_\mathtt{B}}^\top)\mathbf{f}_\mathtt{B}$. ▷ Centralize the boundary mapping $\mathbf{f}_\mathtt{B}$.
27: $\mathbf{f}_\mathtt{B} \leftarrow \operatorname{diag}(|\mathbf{f}_\mathtt{B}|)^{-1}\mathbf{f}_\mathtt{B}$. ▷ Normalize the boundary mapping $\mathbf{f}_\mathtt{B}$.
28: Solve $L_{\mathtt{I},\mathtt{I}}\mathbf{f}_\mathtt{I} = -L_{\mathtt{I},\mathtt{B}}\mathbf{f}_\mathtt{B}$. ▷ Update the interior mapping $\mathbf{f}_\mathtt{I}$.
29: **if** $E_\beta(\mathbf{f}) > E_\beta(\mathbf{h})$ **then**
30: $\mathbf{f} \leftarrow \mathbf{h}$. ▷ Adopt the previous mapping.
31: **break**
32: **end if**
33: **end while**
34: **return** $E_\beta(\mathbf{f})$.
35: **end procedure**

The condition (i) is necessary for the irreducibility of submatrices that appear in Lemma 3.6. The condition (ii) is equivalent to that the mesh contains no leaf faces, i.e., the face that is connected with only one other face. The condition (iii) is to prevent the mapping from degeneration, i.e., the image of the mapping is an interval or a point.

Also, we give the definition of M-matrix [12] and some related lemmas.

DEFINITION 3.2.

(i) A matrix $A \in \mathbb{R}^{m\times n}$ is said to be nonnegative (positive) if all the entries of A are nonnegative (positive).

ETNA
Kent State University and
Johann Radon Institute (RICAM)

(ii) A square matrix $A \in \mathbb{R}^{n\times n}$ is irreducible, if the corresponding graph $\mathcal{G}(A)$ of A is connected.

DEFINITION 3.3. *A matrix $A \in \mathbb{R}^{n\times n}$ is said to be an M-matrix if $A = sI - B$, where B is nonnegative and $s \geq \rho(B)$, where $\rho(B)$ is the spectral radius of B.*

LEMMA 3.4 (Theorem 1.4.10 in [42]). *Suppose $A \in \mathbb{R}^{n\times n}$ is a singular, irreducible M-matrix. Then each principal submatrix of A other than A itself is a nonsingular M-matrix.*

LEMMA 3.5 (Theorem 1.4.7 in [42]). *If $A \in \mathbb{R}^{n\times n}$ is a nonsingular M-matrix, then A^{-1} is a nonnegative matrix. Moreover, if A is irreducible, then A^{-1} is a positive matrix.*

The following lemma plays an important role in the geometric point of view of the matrix products in (3.1).

LEMMA 3.6. *Given a well-conditioned simply connected open mesh $\mathcal{M}$ of n vertices. Let L be a Laplacian matrices of $\mathcal{M}$, defined similar as in (2.3), with positive weights $\{w_{i,j} \,|\, [v_i, v_j] \in \mathcal{E}(\mathcal{M})\}$. Let $\mathtt{I}$ and $\mathtt{B}$ be index sets of interior vertices and boundary vertices of $\mathcal{M}$, respectively. Then each entry of the vectors $-L_{\mathtt{I},\mathtt{I}}^{-1}L_{\mathtt{I},\mathtt{B}}\mathbf{f}_{\mathtt{B}}$ and $-L_{\mathtt{B},\mathtt{B}}^{-1}L_{\mathtt{B},\mathtt{I}}\mathbf{f}_{\mathtt{I}}$ is a convex combination of the entries of $\mathbf{f}_{\mathtt{B}}$ and $\mathbf{f}_{\mathtt{I}}$, respectively.*

Proof. From the definition of the Laplacian matrix (2.3), it is clear that $L\mathbf{1}_n = \mathbf{0}$, i.e.,

$$\begin{cases} L_{\mathtt{I},\mathtt{I}}\mathbf{1}_{n_{\mathtt{I}}} + L_{\mathtt{I},\mathtt{B}}\mathbf{1}_{n_{\mathtt{B}}} = \mathbf{0}, \\ L_{\mathtt{I},\mathtt{B}}^{\top}\mathbf{1}_{n_{\mathtt{I}}} + L_{\mathtt{B},\mathtt{B}}\mathbf{1}_{n_{\mathtt{B}}} = \mathbf{0}. \end{cases} \tag{3.2}$$

Note that L is a singular irreducible M-matrix. By Lemma 3.4, the matrices $L_{\mathtt{I},\mathtt{I}}$ and $L_{\mathtt{B},\mathtt{B}}$ are invertible. Then (3.2) implies that

$$\begin{cases} -L_{\mathtt{I},\mathtt{I}}^{-1}L_{\mathtt{I},\mathtt{B}}\mathbf{1}_{n_{\mathtt{B}}} = \mathbf{1}_{n_{\mathtt{I}}}, \\ -L_{\mathtt{B},\mathtt{B}}^{-1}L_{\mathtt{I},\mathtt{B}}^{\top}\mathbf{1}_{n_{\mathtt{I}}} = \mathbf{1}_{n_{\mathtt{B}}}. \end{cases} \tag{3.3}$$

In addition, from the definition of the Laplacian matrix and the assumption of positive weights, the entries of $-L_{\mathtt{I},\mathtt{B}}$ are non-negative. Furthermore, the irreducibility of $L_{\mathtt{I},\mathtt{I}}$ and $L_{\mathtt{B},\mathtt{B}}$ are, respectively, guaranteed by Definition 3.1 (i) and the simply connected assumption of $\mathcal{M}$. By Lemma 3.5, $L_{\mathtt{I},\mathtt{I}}^{-1}$ and $L_{\mathtt{B},\mathtt{B}}^{-1}$ are positive, so that the entries of the matrices $-L_{\mathtt{I},\mathtt{I}}^{-1}L_{\mathtt{I},\mathtt{B}}$ and $-L_{\mathtt{B},\mathtt{B}}^{-1}L_{\mathtt{B},\mathtt{I}}$ are non-negative. Therefore, (3.3) implies each entry of the vectors $-L_{\mathtt{I},\mathtt{I}}^{-1}L_{\mathtt{I},\mathtt{B}}\mathbf{f}_{\mathtt{B}}$ and $-L_{\mathtt{B},\mathtt{B}}^{-1}L_{\mathtt{B},\mathtt{I}}\mathbf{f}_{\mathtt{I}}$ is a convex combination of the entries of $\mathbf{f}_{\mathtt{B}}$ and $\mathbf{f}_{\mathtt{I}}$, respectively. ∎

Now we prove the existence of nontrivial accumulation vectors of the iterations (3.1) in the following theorem.

THEOREM 3.7. *Suppose the sequence $\{\mathbf{f}_{\mathtt{B}}^{(k)}\}_{k\in\mathbb{N}}$ defined in (3.1) with $L_\beta(f^{(k)})$ satisfying the assumption of Lemma 3.6. Then it has a nontrivial accumulation vector $\mathbf{f}_{\mathtt{B}}^{(*)}$.*

Proof. Since every entry of $\mathbf{f}_{\mathtt{B}}^{(k)}$ is on the unit circle, by Bolzano-Weierstrass theorem there exists a vector $\mathbf{f}_{\mathtt{B}}^{(*)}$ and a convergent subsequence $\{\mathbf{f}_{\mathtt{B}}^{(k_j)}\}_{j\in\mathbb{N}}$ such that

$$\lim_{j\to\infty} \mathbf{f}_{\mathtt{B}}^{(k_j)} = \mathbf{f}_{\mathtt{B}}^{(*)}.$$

From Lemma 3.6, for $\ell = 1, \ldots, n_{\mathtt{I}}$,

$$(\mathbf{f}_{\mathtt{I}}^{(k)})_\ell = -\left(\left[L_\beta(f^{(k)})\right]_{\mathtt{I},\mathtt{I}}^{-1}\left[L_\beta(f^{(k)})\right]_{\mathtt{I},\mathtt{B}}\mathbf{f}_{\mathtt{B}}^{(k)}\right)_\ell$$

is a convex combination of the points $\{(\mathbf{f}_{\mathtt{B}}^{(k)})_\ell\}_{\ell=1}^{n_{\mathtt{B}}} \subset \partial\mathbb{D}$, so that $(\mathbf{f}_{\mathtt{I}}^{(k)})_\ell \in \mathbb{D}$, for $\ell = 1, \ldots, n_{\mathtt{I}}$. It follows that the inverted points $\widetilde{\mathbf{f}}_{\mathtt{I}}^{(k)} = (D_I^{(k)}\mathbf{f}_{\mathtt{I}}^{(k)})_\ell$ are located in $\mathbb{C}\backslash\mathbb{D}$, for

ETNA
Kent State University and
Johann Radon Institute (RICAM)

$\ell = 1, \ldots, n_{\mathtt{I}}$. Again, from Lemma 3.6, for $\ell = 1, \ldots, n_{\mathtt{B}}$,

$$(\widetilde{\mathbf{f}}_{\mathtt{B}}^{(k)})_\ell = -\left(\left[L_\beta(f^{(k)}) \right]_{\mathtt{B},\mathtt{B}}^{-1} \left[L_\beta(f^{(k)}) \right]_{\mathtt{B},\mathtt{I}} \widetilde{\mathbf{f}}_{\mathtt{I}}^{(k)} \right)_\ell$$

is a convex combination of the points $\{(\widetilde{\mathbf{f}}_{\mathtt{I}}^{(k)})_\ell\}_{\ell=1}^{n_{\mathtt{I}}} \subset \mathbb{C}\backslash\mathbb{D}$. As a result, the centralization in the iteration (3.1) guarantees that after a rotation by setting $(\mathbf{f}_{\mathtt{B}}^{(k)})_1 = 1$ for each $k \in \mathbb{N}$, the maximal argument over all $\mathrm{Arg}(C\widetilde{\mathbf{f}}_{\mathtt{B}}^{(k)})_\ell$, for $\ell = 1, \ldots, n_{\mathtt{B}}$, should be greater than π. Otherwise, each entry of the vector $C\widetilde{\mathbf{f}}_{\mathtt{B}}^{(k)}$ is located on the upper half-plane of $\mathbb{C}$. Then the center

$$\frac{1}{n_{\mathtt{B}}} \sum_{\ell=1}^{n_{\mathtt{B}}} (C\widetilde{\mathbf{f}}_{\mathtt{B}}^{(k)})_\ell \neq 0,$$

which contradicts to the fact that the center should be zero. In particular, it holds for the subsequence $\{k_j\}_{j\in\mathbb{N}}$. Hence, the maximal argument over all components of the accumulation point $\mathbf{f}_{\mathtt{B}}^{(*)}$ should be greater than or equal to π. Therefore, $\mathbf{f}_{\mathtt{B}}^{(*)}$ is nontrivial. ∎

THEOREM 3.8. *The mapping* $\mathbf{f}^{(*)} := \begin{bmatrix} \mathbf{f}_{\mathtt{I}}^{(*)} \\ \mathbf{f}_{\mathtt{B}}^{(*)} \end{bmatrix} : \mathcal{M} \to \mathbb{D}$ *constructed by Theorem 3.7 is one-to-one.*

Proof. For convenience, we denote $L_{\mathtt{I},\mathtt{I}} := [L_\beta(\mathbf{f}^{(*)})]_{\mathtt{I},\mathtt{I}}$, $L_{\mathtt{I},\mathtt{B}} = L_{\mathtt{B},\mathtt{I}}^\top := [L_\beta(\mathbf{f}^{(*)})]_{\mathtt{I},\mathtt{B}}$, $L_{\mathtt{B},\mathtt{B}} := [L_\beta(\mathbf{f}^{(*)})]_{\mathtt{B},\mathtt{B}}$ and $D_{\mathtt{I}} := \mathrm{diag}(L_{\mathtt{I},\mathtt{I}})$, $D_{\mathtt{B}} := \mathrm{diag}(L_{\mathtt{B},\mathtt{B}})$. From (2.10), (2.7) and Lemma 3.6 follows that

$$\begin{cases} D_I^{-1}(L_{\mathtt{I},\mathtt{I}}\mathbf{f}_{\mathtt{I}}^{(*)} + L_{\mathtt{I},\mathtt{B}}\mathbf{f}_{\mathtt{B}}^{(*)}) = \mathbf{0}, \\ D_B^{-1}(L_{\mathtt{B},\mathtt{I}}\mathbf{f}_{\mathtt{I}}^{(*)} + L_{\mathtt{B},\mathtt{B}}\mathbf{f}_{\mathtt{B}}^{(*)}) = \mathbf{0}. \end{cases}$$

From (3.2), we have that

$$\begin{cases} 1 - \sum_{j\in N(v_\ell)} \lambda_{\ell,j} \equiv e_\ell^\top (D_I^{-1} L_{\mathtt{I},\mathtt{I}} \mathbf{1}_{n_{\mathtt{I}}} + D_I^{-1} L_{\mathtt{I},\mathtt{B}} \mathbf{1}_{n_{\mathtt{B}}}) = \mathbf{0}, \ \ell \in \mathtt{I}, \\ 1 - \sum_{j\in N(v_\ell)} \lambda_{\ell,j} \equiv e_\ell^\top (D_B^{-1} L_{\mathtt{B},\mathtt{I}} \mathbf{1}_{n_{\mathtt{I}}} + D_B^{-1} L_{\mathtt{B},\mathtt{B}} \mathbf{1}_{n_{\mathtt{B}}}) = \mathbf{0}, \ \ell \in \mathtt{B}, \end{cases}$$

from n convex combinations of one, where $N(v_\ell)$ denotes the 1-ring vertex neighbor of the vertex v_ℓ. This implies that $\mathbf{f}^{(*)}$ is a convex combination map from $\mathcal{M}$ to $\mathbb{D}$ which maps $\partial\mathcal{M}$ homeomorphically into the boundary of the convex hull of $\{\mathbf{f}_\ell^{(*)}\}_{\ell\in\mathtt{B}}$. From Theorem 6.7 of [21] follows that $\mathbf{f}^{(*)}$ is one-to-one. ∎

4. Numerical Experiments. In this section, we demonstrate numerical experiments of the BEM algorithm for balanced parameterizations of simply connected open surfaces. Some of the surface mesh models are obtained from TurboSquid [5], AIM@SHAPE shape repository [3], the Stanford 3D scanning repository [4], a project page of ALICE [1], and Gu's website [2]. All computations in this paper are performed in MATLAB.

To quantify the distortions of the parameterizations computed by the BEM algorithm, we introduce the measurement as follows. The angle distortion is measured by the mean and standard deviation (SD) of the angle difference in degree

$$\mathcal{D}_{\mathrm{angle}}(v, [u, v, w]) = |\angle(u, v, w) - \angle(f(u), f(v), f(w))| \ \text{(degree)}, \tag{4.1}$$

where $v \in \mathcal{V}(\mathcal{M})$ and $[u, v, w] \in \mathcal{F}(\mathcal{M})$. The area distortion is measured by the mean and SD of the area ratio

$$\mathcal{R}_{\mathrm{area}}(v) = \frac{\sum_{\tau\in N(v)} |f(\tau)| / |f(\mathcal{M})|}{\sum_{\tau\in N(v)} |\tau| / |\mathcal{M}|}, \tag{4.2}$$

ETNA
Kent State University and
Johann Radon Institute (RICAM)

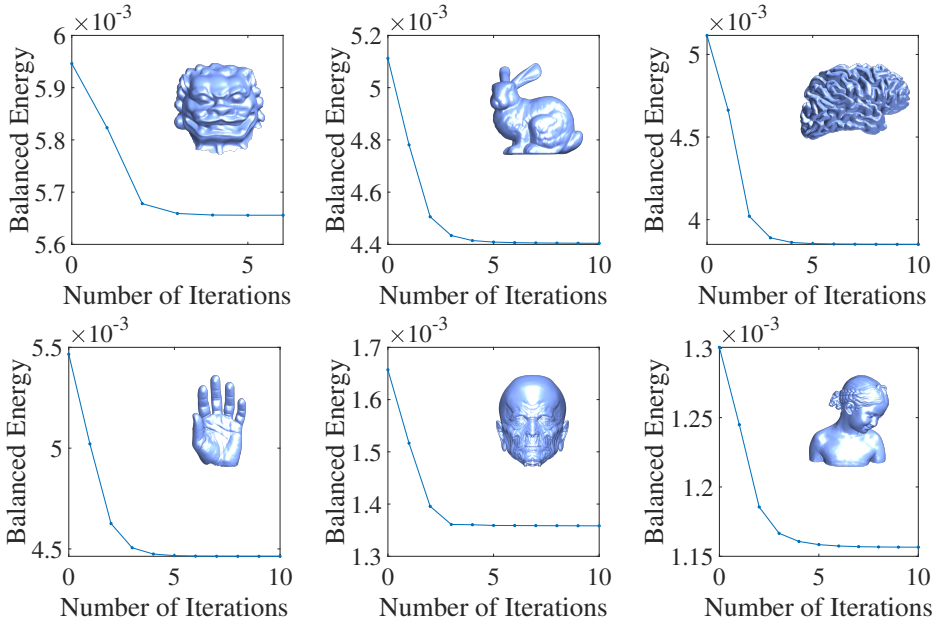

FIG. 4.1. *The relationship between the number of iterations and the balanced energy of the parameterization computed by the BEM algorithm.*

where $v \in \mathcal{V}(\mathcal{M})$, $N(v) = \{\tau \in \mathcal{F}(\mathcal{M}) \,|\, v \subset \tau\}$ is the set of neighboring triangular faces of the vertex v, $|\mathcal{M}|$ and $|f(\mathcal{M})|$ denote areas of $\mathcal{M}$ and its image $f(\mathcal{M})$, respectively.

Table 4.1 shows the optimal balancing coefficient β^* determined by (2.11) and the balanced energy E_{β^*}, as well as the mean and SD of the angle difference $\mathcal{D}_{\text{angle}}$ in (4.1) and the area ratio $\mathcal{R}_{\text{area}}$ in (4.2) of parameterizations, respectively, and the computational cost by the BEM algorithm. From Table 4.1, we observe that both the mean and SD of the angle distortions are roughly 4 to 6 degrees, which is fairly acceptable. In addition, the mean of the area ratios is roughly 1 with the SD being 0.7 to 2.3, which is also relatively acceptable.

Furthermore, Fig. 4.1 shows the relationship between the number of iterations and the balanced energy of the parameterization computed by the BEM algorithm. We can observe that the balanced energy is significantly decreased in the first 3 iteration steps and then slowly convergent, which indicates that the BEM algorithm performs effectively on decreasing the balanced energy. According to the convergence behavior of the the benchmark mesh models in Fig. 4.1, it is sufficient to set the maximal number of iterations s_g in (2.12) to be 10. In addition, the number s_β in (2.12) is between 7–9.

Comparisons of the optimal distortion-balancing parameterizations of the benchmark mesh models [5, 3, 4, 1, 2] computed by the BEM algorithm with the conformal ($\beta = 0$) and equiareal ($\beta = 1$) parameterizations are demonstrated in Fig. 4.2, in which the lighting on the images is based on the normal vectors of the mesh models. We see that the balanced parameterizations ($\beta = \beta^*$) is more close to the conformal parameterization ($\beta = 0$). Furthermore, Figures 4.3 and 4.4 show the angle distortions as well as the absolute value of the logarithm of the area ratios of the parameterizations. From the color bars in Fig. 4.3, we see that the angle distortion of the balanced parameterization is close to the angle-preserving parameterization, but the area-preserving is far from angle preservation. On the other hand, from Fig. 4.4, we observe that the region of yellow color of the balanced parameterization for each mesh model is considerably reduced compared to the angle-preserving parameterization,

ETNA
Kent State University and
Johann Radon Institute (RICAM)

TABLE 4.1
The mean and SD of the angle difference $\mathcal{D}_{\text{angle}}$ in (4.1) and the area ratio $\mathcal{R}_{\text{area}}$ in (4.2) of parameterizations, respectively, as well as the computational cost by the BEM algorithm with balancing coefficients β^*.

Model Name	# Faces	β^*	E_{β^*}	$\mathcal{D}_{\text{angle}}$ (Degree)		$\mathcal{R}_{\text{area}}$		Time
				Mean	SD	Mean	SD	(Sec.)
Chinese Lion	34,421	0.2649	0.0057	4.5252	4.3976	1.0029	0.7534	3.17
Stanford Bunny	65,221	0.3336	0.0044	5.4930	6.2576	0.9772	1.0856	9.37
Human Brain	96,811	0.2127	0.0039	4.3981	4.8866	1.0314	2.3442	19.77
Left Hand	105,860	0.3315	0.0045	4.9991	6.5568	1.0258	1.5960	20.30
Human Head	266,776	0.2570	0.0014	4.6021	4.7208	1.1138	0.8464	24.44
Bimba Statue	836,734	0.4899	0.0012	6.0047	5.9775	0.9486	1.0924	195.14

which means the area distortion of the balanced parameterization is significantly improved. In summary, the BEM algorithm takes into account both advantages of conformal $(\beta = 0)$ and equiareal $(\beta = 1)$.

It is worth noting that among the demonstrated benchmark mesh models, all the balanced parameterization computed by the BEM algorithm are numerically bijective while some of the conformal and equiareal parameterizations are not. Specifically, the conformal parameterizations of Human Head and Bimba Statue contain 1 and 3 folding faces, respectively, and the equiareal parameterization of Stanford Bunny contains 6 folding faces.

5. Applications on 3D Chinese Virtual Broadcasting System. The virtual broadcasting refers to the process of automatically generating the video of broadcasting a given article. With the virtual broadcasting system, the user can easily make a broadcasting video by inputting a few sentences or a paragraph. Due to the fact that the Chinese syllables are composed of 1 to 3 Mandarin phonetic symbols, a Chinese virtual broadcasting system can be realized via recording the videos of pronouncing all the 37 phonetic symbols and construct the in-between smooth homotopy of surfaces. With the aid of the distortion-balancing parameterizations of surfaces obtained by the BEM algorithm, the correspondence between each pair of surfaces can be computed efficiently in the unit disk. Then the in-between motion of each pair of surfaces can be constructed by the linear homotopy. The in-between smooth motion of a surface sequence can be built up by the cubic spline homotopy.

The broadcasting system requires the following key steps. First, in Section 5.1, a remeshing process is introduced to improve the mesh quality of the captured raw surface mesh data. Then a registration process is introduced in Section 5.2 to find a one-to-one correspondence between each pair of surfaces. In Section 5.3, a morphing process is introduced to construct a smooth 3D video sequence for the inputted sequence of surfaces. Furthermore, to obtain a better visual effect, we demonstrate a technique of alignment and fusion in Section 5.4 so that each face is aligned and fused with a half-length portrait.

The importance of BEM algorithm in solving the real applications is summarized as follows.

- The BEM algorithm can numerically produce a bijective parameterization while the conformal $(\beta = 0)$ and the equiareal $(\beta = 1)$ algorithms can not guarantee the bijectivity. See the last paragraph of Section 4.
- The remeshing procedure by applying the BEM algorithm can improve the uniformity of vertex sampling and the quality of right triangles. See Subsection 5.1.
- The virtual broadcasting system is based on the exactness of the registration map, i.e., the one-to-one correspondence, between surfaces in which the mesh quality and the bijectivity of parameterizations are crucial. See Subsection 5.2.

ETNA
Kent State University and
Johann Radon Institute (RICAM)

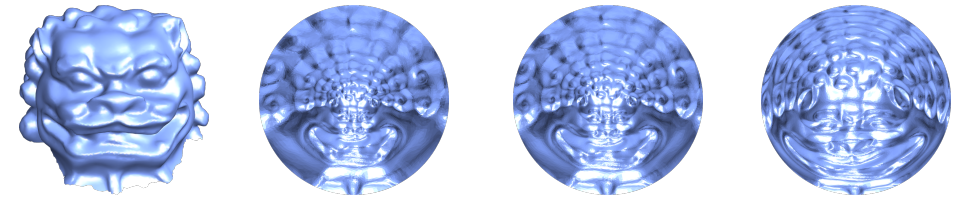

(a) *Chinese Lion* conformal ($\beta = 0$) balanced ($\beta = 0.2649$) equiareal ($\beta = 1$)

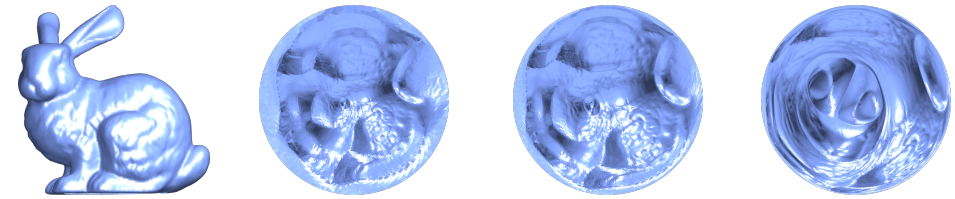

(b) *Stanford Bunny* conformal ($\beta = 0$) balanced ($\beta = 0.3336$) equiareal ($\beta = 1$)

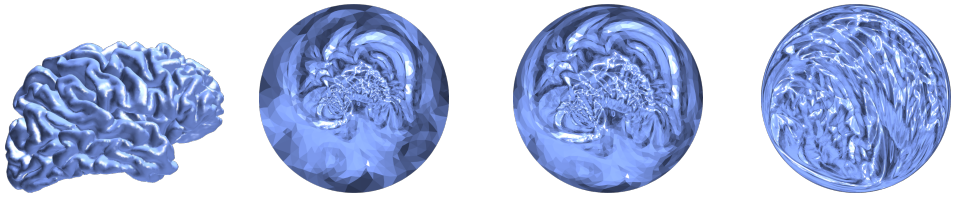

(c) *Human Brain* conformal ($\beta = 0$) balanced ($\beta = 0.2127$) equiareal ($\beta = 1$)

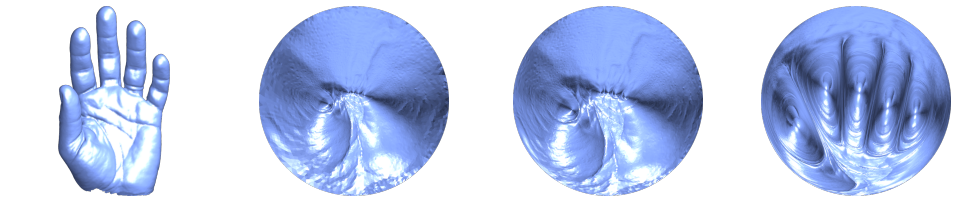

(d) *Left Hand* conformal ($\beta = 0$) balanced ($\beta = 0.3315$) equiareal ($\beta = 1$)

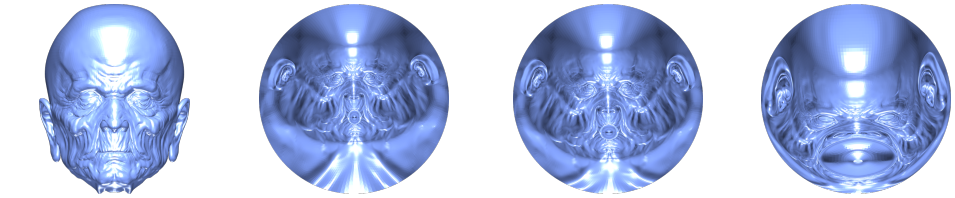

(e) *Human Head* conformal ($\beta = 0$) balanced ($\beta = 0.2570$) equiareal ($\beta = 1$)

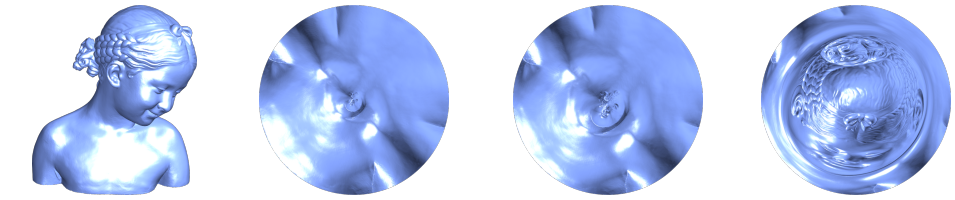

(f) *Bimba Statue* conformal ($\beta = 0$) balanced ($\beta = 0.4899$) equiareal ($\beta = 1$)

FIG. 4.2. *The benchmark mesh models and their conformal, balanced, and equiareal parameterizations.*

ETNA
Kent State University and
Johann Radon Institute (RICAM)

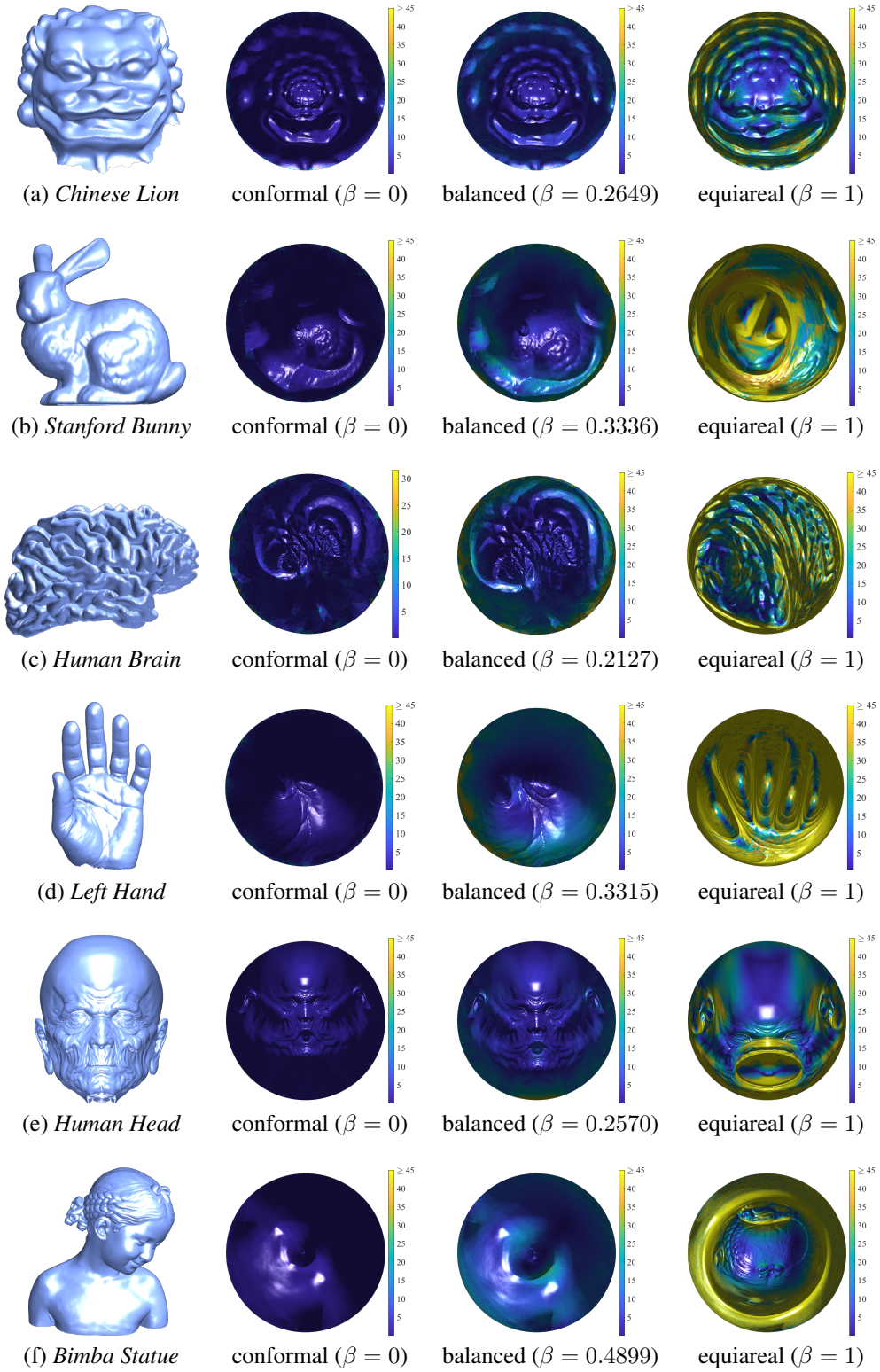

FIG. 4.3. *The benchmark mesh models and the angle distortions of their conformal, balanced, and equiareal parameterizations.*

ETNA
Kent State University and
Johann Radon Institute (RICAM)

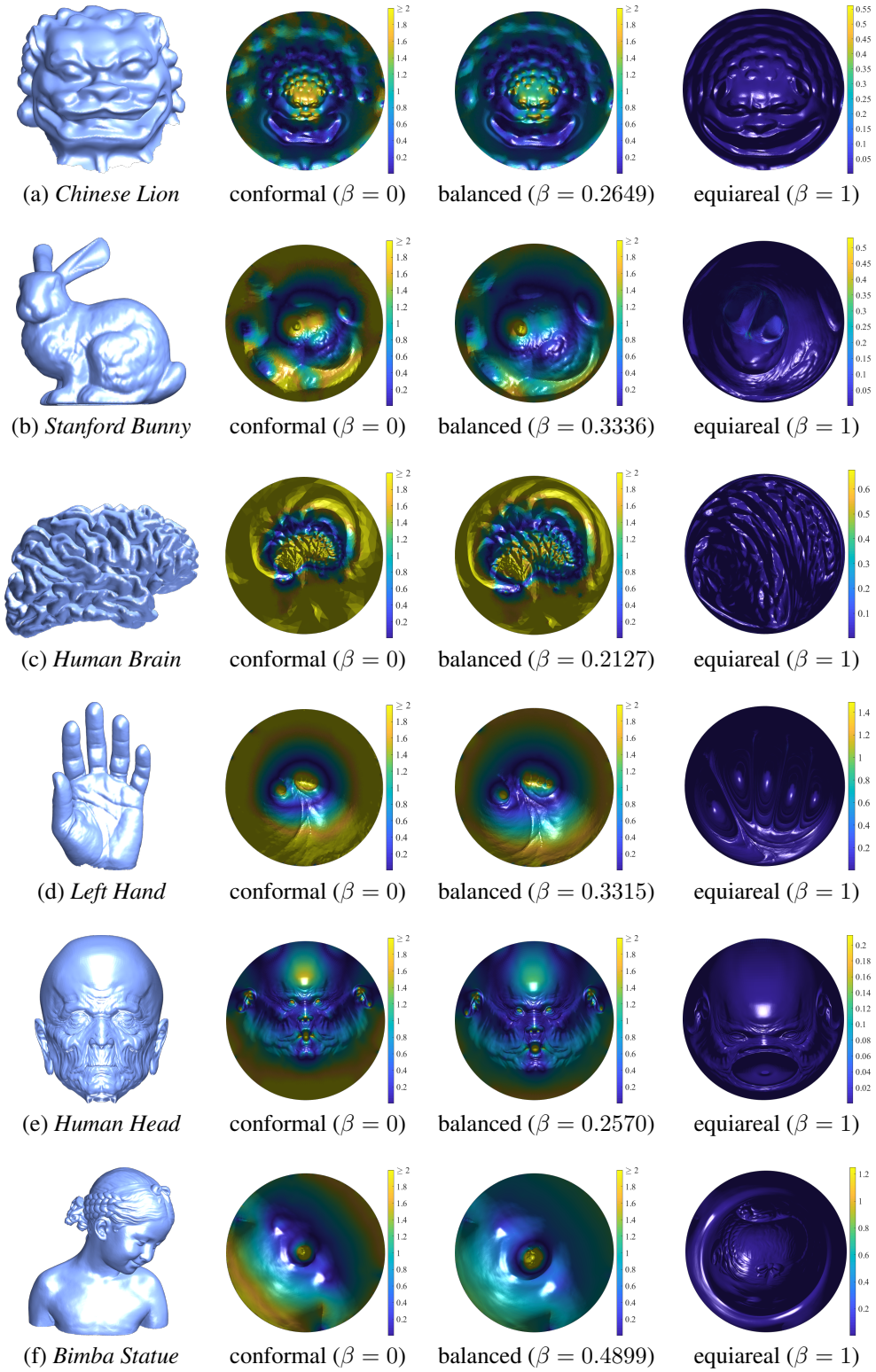

FIG. 4.4. *The benchmark mesh models and the absolute value of the logarithm of the area ratios of their conformal, balanced, and equiareal parameterizations.*

ETNA
Kent State University and
Johann Radon Institute (RICAM)

5.1. Surface Remeshing for Structured-Light Based 3D Scanner. Surface remeshing refers to the improvement process of the mesh quality, including the uniformity of vertex sampling, the regularity of mesh connectivity and the quality of triangles [10, 14]. In particular, the quality of a triangle $[u, v, w]$ can be measured by the quantity

$$\mathcal{Q}([u,v,w]) = \left\| \begin{bmatrix} |[u,v]| \\ |[v,w]| \\ |[w,u]| \end{bmatrix} - \frac{1}{3}\left(|[u,v]| + |[v,w]| + |[w,u]|\right)\mathbf{1}_3 \right\|_2 . \tag{5.1}$$

The smaller the value $\mathcal{Q}(\tau)$, the better the quality of the triangle τ. Note that an equilateral triangle τ has value $\mathcal{Q}(\tau) = 0$.

By applying the BEM algorithm, the remeshing procedure can be smoothly carried out as follows. First, a distortion-balancing parameterization $f : \mathcal{M} \to \mathbb{D} \subset \mathbb{C}$ is computed by the BEM algorithm. Then the image $f(\mathcal{M})$ is covered by a regular mesh $\mathcal{U}$ of a unit disk with uniform sampling. Finally, the remeshed surface $f^{-1}(\mathcal{U})$ is obtained by the one-to-one correspondences between the barycentric coordinates of each triangular face on $\mathcal{M}$ and on $f(\mathcal{M})$.

In our numerical experiments, the raw mesh data of human faces are captured by the structured-light based 3D scanner GeoVideo, manufactured by the Geometric Informatics company, in the ST Yau Center at National Chiao Tung University in Taiwan. Fig. 5.1 shows the histograms of the angles and areas, respectively, as well as the quality of triangles for (a) the raw mesh data and (b)–(d) the remeshed data by the BEM with $\beta = \beta^*$, 0, and 1, respectively, of a human face. It indicates that the mesh quality in terms of regularity of triangles and the uniformity of triangle areas in (b) is the best compared with (a), (c), and (d). Furthermore, we see that the quality $\mathcal{Q}$ in (5.1) of triangles in Fig. 5.1 (b) and (c) is much better than that in (a) and (d).

On the other hand, Fig. 5.2 shows the zoom-in images at the nose part of (a) the raw mesh data and (b) the remeshed data by the BEM ($\beta = \beta^*$) of the human face. We see that there are lots of obtuse triangles at the nose part of (a) while most of the triangles in (b) are close to equilateral triangles.

5.2. Surface Registration. The registration between a pair of surfaces $\mathcal{M}$ and $\mathcal{N}$ refers to developing a feasible algorithm for the computation of a homeomorphism $f : \mathcal{M} \to \mathcal{N}$ that maps $\mathcal{M}$ to $\mathcal{N}$ bijectively such that the characteristics of the surfaces are matched. It is a fundamental issue that has been widely applied to computer graphics and geometry processing [37, 41, 54, 59]. The characteristics of surfaces are often represented as sets of landmarks (feature points). We denote $\mathcal{V}(\mathcal{M}) = \{v_1, v_2, \ldots, v_m\}$ and let $\mathtt{I}$ and $\mathtt{B}$ be the index sets of interior and boundary vertices of $\mathcal{M}$, respectively. Without loss of generality, suppose the index sets of landmarks on the interior and boundary of $\mathcal{M}$ are given by

$$\mathtt{P} = \{\mathtt{P}(1), \mathtt{P}(2), \ldots, \mathtt{P}(n_{\mathtt{P}})\} \text{ and } \mathtt{R} = \{\mathtt{R}(1), \mathtt{R}(2), \ldots, \mathtt{R}(n_{\mathtt{R}})\},$$

respectively, and the coordinates of landmarks on the interior and boundary of $\mathcal{N}$ are given by

$$Q = \{q_1, q_2, \ldots, q_{n_{\mathtt{P}}}\} \text{ and } S = \{s_1, s_2, \ldots, s_{n_{\mathtt{R}}}\},$$

respectively. The goal of the surface registration is to construct a low-distorted bijective mapping $\varphi : \mathcal{M} \to \mathcal{N}$ that satisfies $\varphi(v_{\mathtt{P}(\ell)}) = q_\ell$, for $\ell = 1, 2, \ldots, n_{\mathtt{P}}$, and $\varphi(v_{\mathtt{R}(\ell)}) = s_\ell$, for $\ell = 1, 2, \ldots, n_{\mathtt{R}}$. By applying the distortion-balancing parameterizations

$$f : \mathcal{M} \to \mathbb{D} \quad \text{and} \quad g : \mathcal{N} \to \mathbb{D},$$

ETNA
Kent State University and
Johann Radon Institute (RICAM)

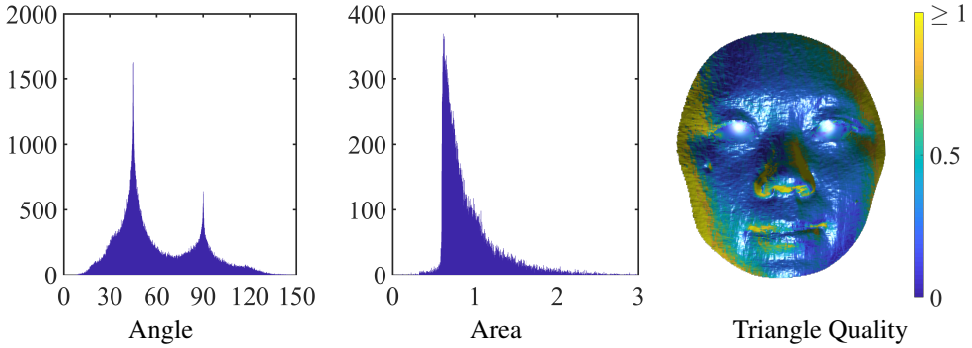

(a) The raw mesh data

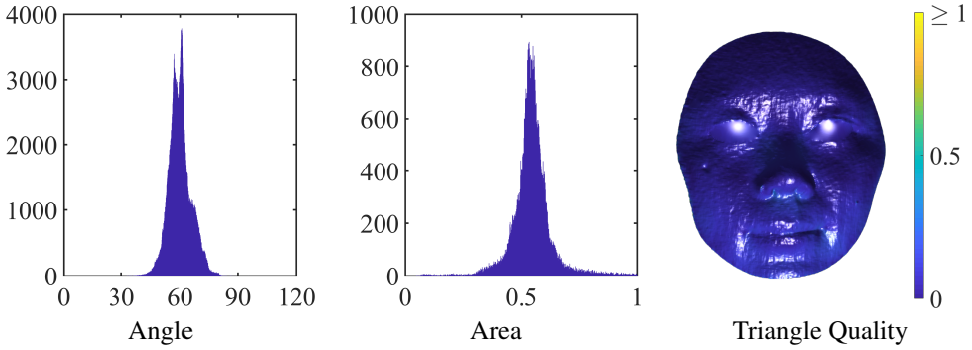

(b) The remeshed data by BEM ($\beta = \beta^*$)

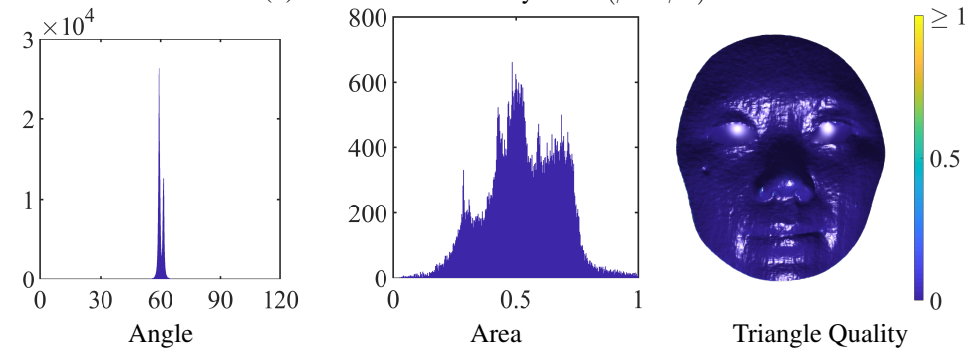

(c) The remeshed data by conformal parameterization ($\beta = 0$)

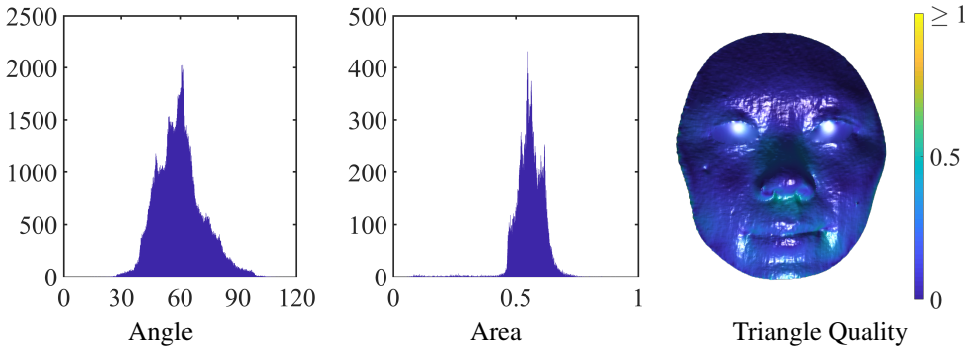

(d) The remeshed data by equiareal parameterization ($\beta = 1$)

FIG. 5.1. *The histograms of the angles and areas, respectively, as well as the quality of triangles for (a) the raw mesh data and (b)–(d) the remeshed data by the BEM with* $\beta = \beta^*$, 0, *and* 1, *respectively, of a human face.*

ETNA
Kent State University and
Johann Radon Institute (RICAM)

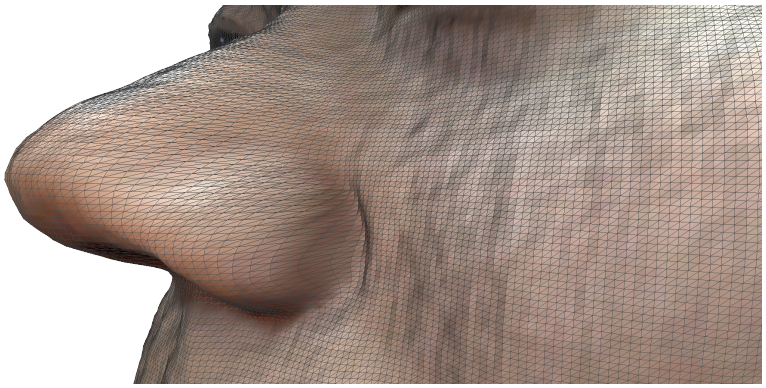

(a) The raw mesh data

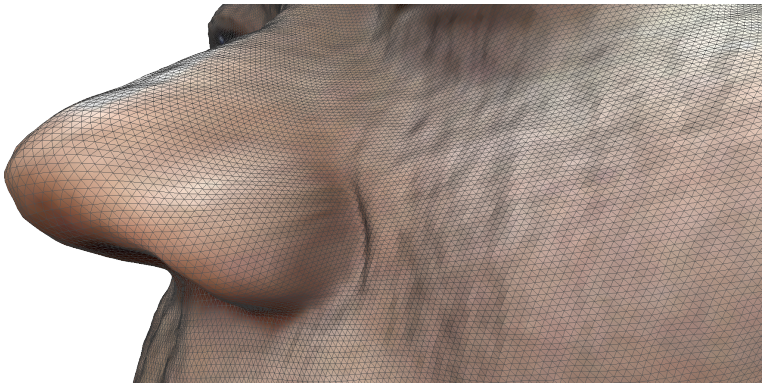

(b) The remeshed data by BEM ($\beta = \beta^*$)

FIG. 5.2. *The zoom-in images at the nose part of (a) the raw mesh data and (b) the remeshed data by BEM* ($\beta = \beta^*$) *of a human face.*

the surface registration in $\mathbb{R}^3$ is reduced into a planar registration on $\mathbb{D}$. The reduced issue is to find a low-distorted bijective mapping $h : \mathbb{D} \to \mathbb{D}$ that satisfies

$$h \circ f(v_{\mathtt{P}(\ell)}) = g(q_\ell), \quad \text{for } \ell = 1, \ldots, n_{\mathtt{P}},$$

and

$$h \circ f(v_{\mathtt{R}(\ell)}) = g(s_\ell), \quad \text{for } \ell = 1, \ldots, n_{\mathtt{R}}.$$

Once we have such a mapping h, the mapping $\varphi : \mathcal{M} \to \mathcal{N}$ can be obtained by the composition mapping $\varphi = g^{-1} \circ h \circ f$.

Let the vector $\mathbf{h} = (h(v_1), \ldots, h(v_m))^\top \in \mathbb{C}^m$ represent the piecewise affine map h. Then, the low-distorted registration mapping $h : \mathbb{D} \to \mathbb{D}$ can be obtained by minimizing the penalized biharmonic energy defined as

$$E_P(h) = \|L_H(h)\,\mathbf{h}\|_2^2 + \lambda^2 \sum_{\ell=1}^{n_{\mathtt{P}}} |\mathbf{h}_{\mathtt{P}(\ell)} - g(q_\ell)|^2, \tag{5.2}$$

ETNA
Kent State University and
Johann Radon Institute (RICAM)

in which $\lambda^2 \in (0,\infty)$ is the weight for the penalty, $L_H(h)$ is the Laplacian matrix defined by

$$[L_H(h)]_{i,j} = \begin{cases} -\frac{1}{2}\left(\cot\left(\theta_{i,j}(h)\right) + \cot\left(\theta_{j,i}(h)\right)\right) & \text{if } [v_i, v_j] \in \mathcal{E}(\mathcal{M}), \\ \sum_{\ell \neq i} -[L_H(h)_{i,\ell}] & \text{if } j = i, \\ 0 & \text{otherwise} \end{cases}$$

with $\theta_{i,j}(h)$ and $\theta_{j,i}(h)$ being two angles opposite to the edge $h\left([v_i, v_j]\right)$ connecting points $h(v_i)$ and $h(v_j)$ on $\mathbb{C}$.

The surface registration process is performed as follows. First, the boundary mapping $\mathbf{h}_{\mathtt{B}}$ is chosen to be the unique piecewise affine mapping that satisfies $h \circ f(v_{\mathtt{R}(\ell)}) = g(s_\ell)$, for $\ell = 1, \ldots, n_{\mathtt{R}}$. Then an initial interior mapping $\mathbf{h}_{\mathtt{I}}^{(0)}$ is computed by a harmonic mapping

$$[L_H(f)]_{\mathtt{I},\mathtt{I}} \mathbf{h}_{\mathtt{I}}^{(0)} = -[L_H(f)]_{\mathtt{I},\mathtt{B}} \mathbf{h}_{\mathtt{B}},$$

where f is the distortion-balancing parameterization computed by the BEM algorithm. Next, the penalized biharmonic energy (5.2) is minimized by the iterative procedure

$$\mathbf{h}^{(k+1)} = \underset{\text{given } \mathbf{h}_{\mathtt{B}}}{\operatorname{argmin}} \left(\left\| L_H(h^{(k)})\, \mathbf{h} \right\|_2^2 + \lambda_k^2 \sum_{\ell=1}^{n_{\mathtt{P}}} |\mathbf{h}_{\mathtt{P}(\ell)} - g(q_\ell)|^2 \right), \tag{5.3}$$

which is a standard least squares problem that can be easily solved by the built-in backslash operator $(\backslash)$ in MATLAB. The value of λ_k^2 can be chosen to be sufficiently small so that the resulting mapping is bijective. In practice, the coefficients λ_k^2 in (5.2) are chosen to be a sequence in $(0, 1]$, e.g., $\lambda_k = 0.2$, for $k = 1, \ldots, 10$ and $\lambda_k = 0.4$, for $k = 11, \ldots, 20$, etc.

Fig. 5.3 (a)–(d) show the human faces of 4 different mouth shapes, (e)–(h) show the images of their distortion-balancing parameterizations computed by the BEM algorithm, and (i)–(k) show the images of their registration mappings. In particular, we choose the face $\mathcal{N}$, shown in Fig. 5.3 (a), as the standard face. The balanced parameterization of $\mathcal{N}$ is denoted by g. The green circles on the disks $g(\mathcal{N})$, $f_1(\mathcal{M}_1)$, $f_2(\mathcal{M}_2)$, $f_3(\mathcal{M}_3)$, shown in Fig. 5.3 (e)–(h), are the landmarks of the standard face $\mathcal{N}$ while the red dots on the disks $f_1(\mathcal{M}_1)$, $f_2(\mathcal{M}_2)$, $f_3(\mathcal{M}_3)$, shown in Fig. 5.3 (f)–(h), are the landmarks of the faces $\mathcal{M}_1, \mathcal{M}_2, \mathcal{M}_3$, respectively. From the registration mappings, shown in Fig. 5.3 (i)–(k), we observe that the images of the disks $h_\ell \circ f_\ell(\mathcal{M}_\ell)$ looks similar as the images $f_\ell(\mathcal{M}_\ell)$, for $\ell = 1, 2, 3$, but each red dot is mapped into the corresponding green circle, respectively. Here, the maps $\{h_\ell\}_{\ell=1}^3$ are computed by the iterative procedure (5.3). This indicates that the introduced disk registration performs accurately on mapping the landmarks to the targets while retaining the distortion small.

5.3. Surface Morphing and Virtual Broadcasting. A *morphing* between two surfaces refers to the process of continuously deforming one surface into another one [38, 56]. The correspondence between surfaces plays a crucial role. For example, suppose two surfaces $\mathcal{M}_0$ and $\mathcal{M}_1$ together with a registration mapping $\varphi_1 : \mathcal{M}_0 \to \mathcal{M}_1$ are given. The in-between surfaces $\mathcal{H} : [0, 1] \times \mathcal{M}_0 \to \mathbb{R}^3$ that satisfies $\mathcal{H}(0, \mathcal{M}_0) = \mathcal{M}_0$ and $\mathcal{H}(1, \mathcal{M}_0) = \mathcal{M}_1$ can be obtained by the linear homotopy

$$\mathcal{H}(t, v) = (1 - t)v + t\, \varphi_1(v).$$

In general, suppose $T + 1$ surfaces $\mathcal{M}_0, \ldots, \mathcal{M}_T$ and registration mappings $\varphi_t : \mathcal{M}_0 \to \mathcal{M}_t$, $t = 1, \ldots, T$, are given. Note that the remeshing procedure guarantees that the triangulation of surfaces $\mathcal{M}_0, \ldots, \mathcal{M}_T$ are identical. A smooth morphing sequence between these surfaces can be obtained by a suitable homotopy $\mathcal{H} : [0, T] \times \mathcal{M}_0 \to \mathbb{R}^3$ satisfying

$$\mathcal{H}(0, v) = v \;\text{ and }\; \mathcal{H}(t, v) = \varphi_t(v), \;\text{ for } t = 1, \ldots, T,$$

ETNA
Kent State University and
Johann Radon Institute (RICAM)

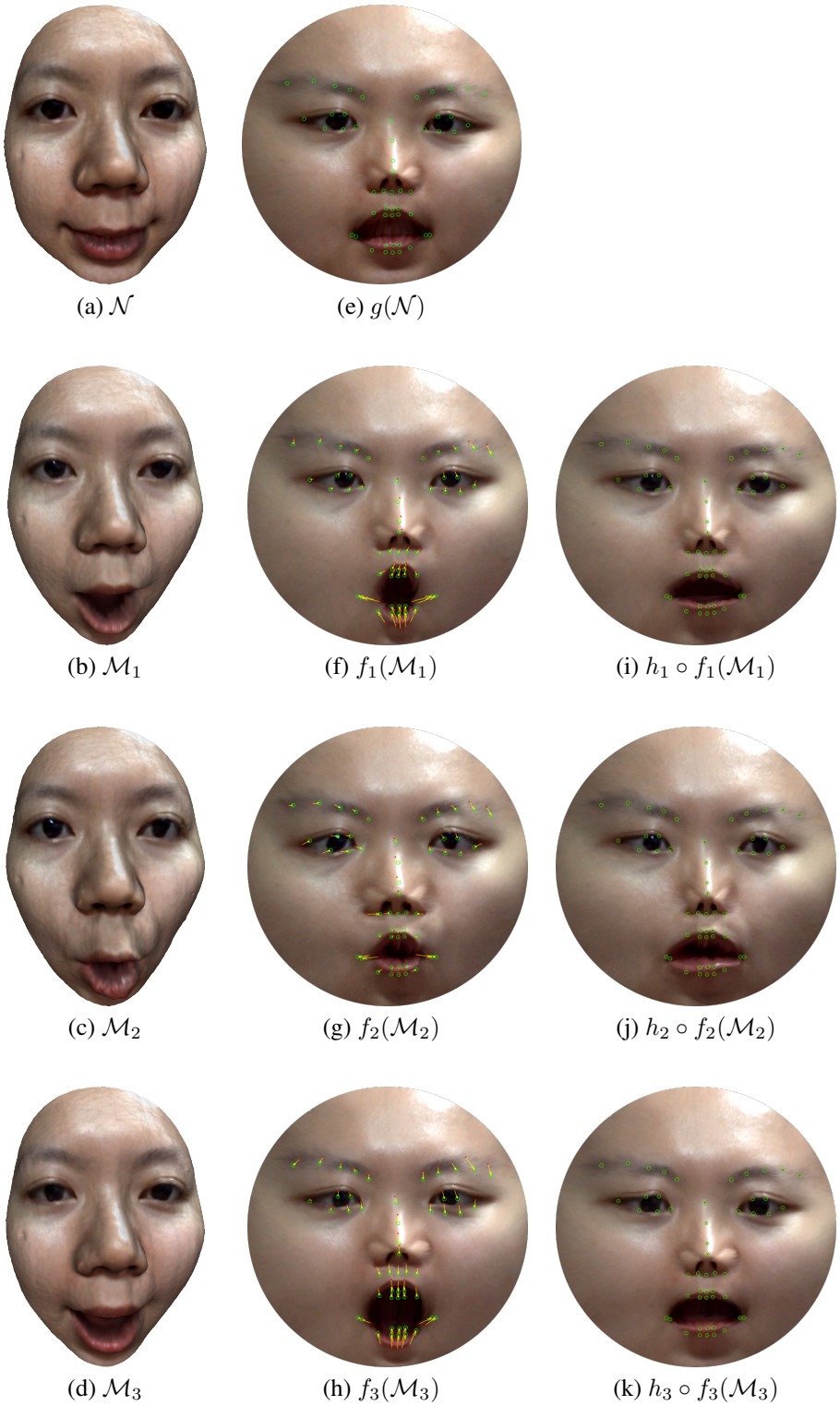

FIG. 5.3. *The registration mappings between human faces of* 4 *different mouth shapes (a)–(d) via the distortion-balancing parameterizations.*

ETNA
Kent State University and
Johann Radon Institute (RICAM)

(a) Head Model (b) Face Surface (c) Fused Model

FIG. 5.4. *(a) The head model obtained from Sketchfab; (b) The face surface captured by the 3D scanner GeoVIdeo; (c) The fused model.*

which can be carried out by a smooth interpolation between the data points

$$\{(0, v), (1, \varphi_1(v)), \ldots, (T, \varphi_T(v)) \mid v \in \mathcal{M}_0\}.$$

Here we adopt the *piecewise cubic Hermite interpolating polynomial* [24] to obtain the homotopy path, which can be easily done by the built-in function `pchip` in MATLAB. A demo video of the Chinese virtual broadcasting of the poem "Yu Mei Ren" can be found at https://mhyueh.github.io/projects/Diskmap_BEM.html.

REMARK 5.1. We apologize for those readers who do not speak Chinese. However, readers can see the changes of mouth-shapes in the video for simulating the pronunciation of Chinese poem.

5.4. Head-Face Alignment and Fusion. The alignment and fusion refer to aligning two or more surface patches into correct positions and fusing them together into one surface. In particular, we focus on the alignment and fusion of the human head and face, e.g., given a head model $\mathcal{M}$ and a human face surface $\mathcal{N}$, as shown in Fig. 5.4 (a) and (b), respectively. The goal is to smoothly align and fuse the head and face together so that the face part of the head model is replaced by the human face surface, as shown in Fig. 5.4 (c).

Let $V_{\mathcal{M}}^{(0)} = \begin{bmatrix} v_1 & v_2 & \cdots & v_n \end{bmatrix}^\top \in \mathbb{R}^{n\times 3}$ be the vertex matrix of $\mathcal{M}$ with the ℓth row being $v_\ell^\top$, for $\ell = 1, \ldots, n$. Let the index set of landmarks on $\mathcal{M}$ be $\mathtt{P}$, and the coordinates of landmarks on $\mathcal{N}$ be $q_1, q_2, \ldots, q_{n_\mathtt{P}} \in \mathbb{R}^3$. The alignment of $\mathcal{M}$ with $\mathcal{N}$ can be carried out by the following procedures. First, the head model $\mathcal{M}$ is appropriately deformed in order to fit with the scanned human face $\mathcal{N}$. The deformed shape of the head model can be computed iteratively by minimizing the change of the mean curvature vectors of $\mathcal{M}$ with a landmark-based penalty [9]

$$V_{\mathcal{M}}^{(k+1)} = \underset{V\in\mathbb{R}^{n\times 3}}{\operatorname{argmin}} \left(\|L_D(V - V_{\mathcal{M}}^{(k)})\|_2^2 + \lambda^2 \sum_{\ell=1}^{n_\mathtt{P}} \|v_{\mathtt{P}(\ell)} - q_\ell\|^2 \right), \tag{5.4}$$

where, in practice, the coefficient λ^2 is chosen to be 0.03. The problem (5.4) can be easily solved by using the least squares method. Next, we let $\mathcal{S} \subset \mathcal{M}$ be the face part of the head model $\mathcal{M}$. Note that both $\mathcal{S}$ and $\mathcal{N}$ are simply connected open triangular meshes. The registration mapping $f : \mathcal{S} \to \mathcal{N}$ can be computed similar as in Section 5.2. Finally, each

ETNA
Kent State University and
Johann Radon Institute (RICAM)

vertex v_ℓ on $\mathcal{S}$ is replaced by

$$v_\ell \leftarrow w_\ell v_\ell + (1 - w_\ell) f(v_\ell),$$

where $w_\ell = 1 - \left(\frac{\mathrm{d}(v_\ell, \partial\mathcal{S})}{\max_\ell \mathrm{d}(v_\ell, \partial\mathcal{S})} \right)^2$ is the weight of quadratically decay function with d being the distance function.

A demo video of the head-face alignment and fusion can be found at https://mhyueh.github.io/projects/Diskmap_BEM.html.

6. Concluding Remarks. In this paper, we propose an efficient BEM algorithm for the computation of optimal distortion-balancing disk-shaped parameterizations of simply connected open surfaces. In addition, we prove the existence of a nontrivial accumulation function of our BEM algorithm under some mild conditions on the triangular mesh and show the limiting function is a bijective map. Applications on the 3D Chinese virtual broadcasting system as well as the head-face alignment and fusion are demonstrated to show the usefulness of the BEM algorithm.

Acknowledgments. The authors want to thank Prof. Chin-Tien Wu for many valuable discussions. M.-H. Yueh was partially supported by MoST 107-2115-M-003-012-. T. Li was supported in parts by the National Natural Science Foundation of China (NSFC) 11971105. W.-W. Lin was partially supported by MoST 106-2628-M-009-004-. This work was partially supported by the Ministry of Science and Technology, the National Center for Theoretical Sciences, the ST Yau Centers in National Chiao Tung University, the Shing-Tung Yau Center of Southeast University, and the Center of Mathematical Sciences and Applications at Harvard University.

REFERENCES

[1] ALICE. http://alice.loria.fr/. Accessed 5 July 2016.
[2] David Xianfeng Gu's Home Page. http://www3.cs.stonybrook.edu/~gu/. Accessed 10 July 2017.
[3] Digital Shape Workbench - Shape Repository. http://visionair.ge.imati.cnr.it/ontologies/shapes/. Accessed 5 July 2016.
[4] The Stanford 3D Scanning Repository. http://graphics.stanford.edu/data/3Dscanrep/. Accessed 23 July 2016.
[5] TurboSquid. http://www.turbosquid.com/. Accessed 23 July 2016.
[6] N. Aigerman, S. Z. Kovalsky, and Y. Lipman. Spherical orbifold tutte embeddings. *ACM Trans. Graph.*, 36(4):90:1–90:13, July 2017.
[7] N. Aigerman and Y. Lipman. Orbifold tutte embeddings. *ACM Trans. Graph.*, 34(6):190:1–190:12, Oct. 2015.
[8] N. Aigerman and Y. Lipman. Hyperbolic orbifold tutte embeddings. *ACM Trans. Graph.*, 35(6):217:1–217:14, Nov. 2016.
[9] M. Alexa and A. Nealen. Mesh editing based on discrete laplace and poisson models. In J. Braz, A. Ranchordas, H. Araújo, and J. Jorge, editors, *Advances in Computer Graphics and Computer Vision*, pages 3–28, Berlin, Heidelberg, 2007. Springer Berlin Heidelberg.
[10] P. Alliez, G. Ucelli, C. Gotsman, and M. Attene. *Recent Advances in Remeshing of Surfaces*, pages 53–82. Springer Berlin Heidelberg, Berlin, Heidelberg, 2008.
[11] S. Angenent, S. Haker, A. Tannenbaum, and R. Kikinis. On the Laplace-Beltrami operator and brain surface flattening. *IEEE Trans. Med. Imaging*, 18(8):700–711, 1999.
[12] A. Berman and R. Plemmons. *Nonnegative Matrices in the Mathematical Sciences*. Society for Industrial and Applied Mathematics, 1994.
[13] R. P. Brent. *Algorithms for Minimization without Derivatives*. Englewood Cliffs, NJ: Prentice-Hall, 1973.
[14] C. P. Choi, X. Gu, and L. M. Lui. Subdivision connectivity remeshing via Teichmüller extremal map. *Inverse Probl. Imag.*, 11(1930-8337_2017_5_825):825, 2017.
[15] G. P.-T. Choi and L. M. Lui. A linear formulation for disk conformal parameterization of simply-connected open surfaces. *Adv. Comput. Math.*, pages 1–28, 2017.
[16] G. P. T. Choi and C. H. Rycroft. Density-equalizing maps for simply connected open surfaces. *SIAM J. Imaging Sci.*, 11(2):1134–1178, 2018.

ETNA
Kent State University and
Johann Radon Institute (RICAM)

[17] P. T. Choi, K. C. Lam, and L. M. Lui. FLASH: Fast landmark aligned spherical harmonic parameterization for genus-0 closed brain surfaces. *SIAM J. Imaging Sci.*, 8(1):67–94, 2015.
[18] P. T. Choi and L. M. Lui. Fast disk conformal parameterization of simply-connected open surfaces. *J. Sci. Comput.*, 65(3):1065–1090, Dec 2015.
[19] P. Degener, J. Meseth, and R. Klein. An adaptable surface parameterization method. In *In Proceedings of the 12th International Meshing Roundtable*, pages 201–213, 2003.
[20] M. Desbrun, M. Meyer, and P. Alliez. Intrinsic parameterizations of surface meshes. *Comput. Graph. Forum*, 21(3):209–218, 2002.
[21] M. S. Floater. One-to-one piecewise linear mappings over triangulations. *Math. Comput.*, 72(242):685–696, 2003.
[22] M. S. Floater and K. Hormann. Surface parameterization: a tutorial and survey. In *Advances in Multiresolution for Geometric Modelling*, pages 157–186. Springer Berlin Heidelberg, 2005.
[23] G. E. Forsythe, M. A. Malcolm, and C. B. Moler. *Computer Methods for Mathematical Computations*. Englewood Cliffs, NJ: Prentice Hall, 1976.
[24] F. N. Fritsch and R. E. Carlson. Monotone piecewise cubic interpolation. *SIAM J. Numer. Anal.*, 17(2):238–246, 1980.
[25] D. X. Gu, F. Luo, and S.-T. Yau. Fundamentals of computational conformal geometry. *Math. Comput. Sci.*, 4(4):389–429, 2010.
[26] X. Gu, Y. Wang, T. F. Chan, P. M. Thompson, and S.-T. Yau. Genus zero surface conformal mapping and its application to brain surface mapping. *IEEE Trans. Med. Imaging*, 8:949–958, 2004.
[27] X. Gu and S.-T. Yau. Computing conformal structures of surfaces. *Communications in Information and Systems*, 2(2):121–146, 2002.
[28] X. Gu and S.-T. Yau. Global conformal surface parameterization. In L. Kobbelt, P. Schroeder, and H. Hoppe, editors, *Eurographics Symposium on Geometry Processing*, SGP '03, pages 127–137, 2003.
[29] X. D. Gu, W. Zeng, F. Luo, and S.-T. Yau. Numerical computation of surface conformal mappings. *Comput. Methods Funct. Theory*, 11(2):747–787, 2011.
[30] S. Haker, S. Angenent, A. Tannenbaum, R. Kikinis, G. Sapiro, and M. Halle. Conformal surface parameterization for texture mapping. *IEEE Trans. Vis. Comput. Graph.*, (2):181–189, 2000.
[31] K. Hormann. Mips: An efficient global parametrization method. In *ACM Press/Addison-Wesley Publishing Co*, 2000.
[32] K. Hormann, B. Lévy, and A. Sheffer. Mesh parameterization: Theory and practice. In *ACM SIGGRAPH Course Notes*, 2007.
[33] W.-Q. Huang, X. D. Gu, T.-M. Huang, S.-S. Lin, W.-W. Lin, and S.-T. Yau. High performance computing for spherical conformal and Riemann mappings. *Geom. Imag. Comput.*, 1(2):223–258, 2014.
[34] W.-Q. Huang, X. D. Gu, W.-W. Lin, and S.-T. Yau. A novel symmetric skew-Hamiltonian isotropic Lanczos algorithm for spectral conformal parameterizations. *J. Sci. Comput.*, 61(3):558–583, Dec 2014.
[35] M. Jin, J. Kim, F. Luo, and X. Gu. Discrete surface ricci flow. *IEEE Trans. Vis. Comput. Graphics*, 14(5):1030–1043, Sep. 2008.
[36] M. Jin, Y. Wang, S.-T. Yau, and X. Gu. Optimal global conformal surface parameterization. In *IEEE Visualization 2004*, pages 267–274, Oct. 2004.
[37] K. C. Lam and L. M. Lui. Landmark- and intensity-based registration with large deformations via quasi-conformal maps. *SIAM J. Imaging Sci.*, 7(4):2364–2392, 2014.
[38] K. C. Lam, C. Wen, and L. M. Lui. Conformal-based surface morphing and multi-scale representation. *Axioms*, 3(2):222–243, 2014.
[39] B. Lévy, S. Petitjean, N. Ray, and J. Maillot. Least squares conformal maps for automatic texture atlas generation. *ACM Trans. Graph.*, 21(3):362–371, July 2002.
[40] L. Liu, L. Zhang, Y. Xu, C. Gotsman, and S. J. Gortler. A local/global approach to mesh parameterization. *Comput. Graphics Forum*, 2008.
[41] L. M. Lui, K. C. Lam, S.-T. Yau, and X. Gu. Teichmuller mapping (t-map) and its applications to landmark matching registration. *SIAM J. Imaging Sci.*, 7(1):391–426, 2014.
[42] J. J. Molitierno. *Applications of Combinatorial Matrix Theory to Laplacian Matrices of Graphs*. CRC Press, 2012.
[43] P. Mullen, Y. Tong, P. Alliez, and M. Desbrun. Spectral conformal parameterization. *Comput. Graph. Forum*, 27(5):1487–1494, 2008.
[44] M. Rabinovich, R. Poranne, D. Panozzo, and O. Sorkine-Hornung. Scalable locally injective mappings. *ACM Trans. Graphics*, 36(2):16:1–16:16, Apr. 2017.
[45] P. V. Sander, J. Snyder, S. J. Gortler, and H. Hoppe. Texture mapping progressive meshes. In *Proceedings of the 28th Annual Conference on Computer Graphics and Interactive Techniques*, SIGGRAPH '01, pages 409–416, New York, NY, USA, 2001. ACM.
[46] R. Sawhney and K. Crane. Boundary first flattening. *ACM Trans. Graph.*, 37(1):5:1–5:14, Dec. 2017.
[47] A. Sheffer and E. de Sturler. Parameterization of faceted surfaces for meshing using angle-based flattening. *Eng. with Comput.*, 17(3):326–337, 2001.

ETNA
Kent State University and
Johann Radon Institute (RICAM)

[48] A. Sheffer, B. Lévy, M. Mogilnitsky, and A. Bogomyakov. ABF++: Fast and robust angle based flattening. *ACM Trans. Graph.*, 24(2):311–330, 2005.

[49] A. Sheffer, E. Praun, and K. Rose. Mesh parameterization methods and their applications. *Found. Trends. Comp. Graphics and Vision.*, 2(2):105–171, 2006.

[50] B. Springborn, P. Schröder, and U. Pinkall. Conformal equivalence of triangle meshes. *ACM Trans. Graph.*, 27(3):77:1–77:11, Aug. 2008.

[51] K. Su, W. Chen, N. Lei, J. Zhang, K. Qian, and X. Gu. Volume preserving mesh parameterization based on optimal mass transportation. *Comput. Aided Design*, 82:42–56, 2017.

[52] K. Su, L. Cui, K. Qian, N. Lei, J. Zhang, M. Zhang, and X. D. Gu. Area-preserving mesh parameterization for poly-annulus surfaces based on optimal mass transportation. *Comput. Aided Geom. D.*, 46:76–91, 2016.

[53] Z. Wang, Z.-x. Luo, J.-l. Zhang, and E. Saucan. ARAP++: an extension of the local/global approach to mesh parameterization. *Frontiers of Information Technology & Electronic Engineering*, 17(6):501–515, Jun 2016.

[54] Y. Yoshiyasu, W.-C. Ma, E. Yoshida, and F. Kanehiro. As-conformal-as-possible surface registration. *Comput. Graph. Forum*, 33(5):257–267, Aug. 2014.

[55] S. Yoshizawa, A. Belyaev, and H. P. Seidel. A fast and simple stretch-minimizing mesh parameterization. In *Proceedings Shape Modeling Applications, 2004.*, pages 200–208, June 2004.

[56] M.-H. Yueh, X. D. Gu, W.-W. Lin, C.-T. Wu, and S.-T. Yau. Conformal surface registration with applications on face morphing. 2016. mathscidoc:1605.09001.

[57] M.-H. Yueh, T. Li, W.-W. Lin, and S.-T. Yau. A novel algorithm for volume-preserving parameterizations of 3-manifolds. *SIAM J. Imag. Sci.*, 12(2):1071–1098, 2019.

[58] M.-H. Yueh, W.-W. Lin, C.-T. Wu, and S.-T. Yau. An efficient energy minimization for conformal parameterizations. *J. Sci. Comput.*, 73(1):203–227, 2017.

[59] M.-H. Yueh, W.-W. Lin, C.-T. Wu, and S.-T. Yau. A novel stretch energy minimization algorithm for equiareal parameterizations. *J. Sci. Comput.*, 78(3):1353–1386, Mar 2019.

[60] R. Zayer, B. Lévy, and H.-P. Seidel. Linear angle based parameterization. In *Proceedings of the Fifth Eurographics Symposium on Geometry Processing*, SGP '07, pages 135–141, Aire-la-Ville, Switzerland, Switzerland, 2007. Eurographics Association.

[61] M. Zhang, R. Guo, W. Zeng, F. Luo, S.-T. Yau, and X. Gu. The unified discrete surface ricci flow. *Graphical Models*, 76(5):321–339, 2014. Geometric Modeling and Processing 2014.

[62] H. Zhao, X. Li, H. Ge, N. Lei, M. Zhang, X. Wang, and X. Gu. Conformal mesh parameterization using discrete Calabi flow. *Comput. Aided Geom. Des.*, 63:96–108, 2018.

[63] X. Zhao, Z. Su, X. D. Gu, A. Kaufman, J. Sun, J. Gao, and F. Luo. Area-preservation mapping using optimal mass transport. *IEEE Trans. Visual Comput. Graphics*, 19(12):2838–2847, Dec 2013.

[64] G. Zou, J. Hu, X. Gu, and J. Hua. Authalic parameterization of general surfaces using Lie advection. *IEEE Transactions on Visualization and Computer Graphics*, 17(12):2005–2014, Dec. 2011.